72-14,974

REITER, Leon, 1931-
RAYLEIGH WAVE ATTENUATION IN THE 15 TO 50 SECOND PERIOD RANGE AND REGIONAL MODELS OF THE INTRINSIC ATTENUATION OF SHEAR WAVES IN THE CRUST AND UPPERMOST MANTLE OF NORTH AMERICA.

The University of Michigan, Ph.D., 1971
Geophysics

University Microfilms, A XEROX Company, Ann Arbor, Michigan

THIS DISSERTATION HAS BEEN MICROFILMED EXACTLY AS RECEIVED

RAYLEIGH WAVE ATTENUATION IN THE 15 TO 50 SECOND PERIOD RANGE AND REGIONAL MODELS OF THE INTRINSIC ATTENUATION OF SHEAR WAVES IN THE CRUST AND UPPERMOST MANTLE OF NORTH AMERICA

by

Leon Reiter

A dissertation submitted in partial fulfillment
of the requirements for the degree of
Doctor of Philosophy
(Geology)
in The University of Michigan
1971

Doctoral Committee:

Professor James T. Wilson, Chairman
Assistant Professor Bruce R. Clark
Professor Ivor K. McIvor
Associate Professor Henry N. Pollack
Professor Paul W. Pomeroy

PLEASE NOTE:

Some pages have indistinct
print. Filmed as received.

University Microfilms, A Xerox Education Company

ACKNOWLEDGMENTS

I would like to thank Professors James T. Wilson and Henry N. Pollack who at different times served as chairman of my doctoral committee and offered me direction and assistance in achieving my educational goals. They and Professors Bruce R. Clark and Ivor K. McIvor read this manuscript critically and offered many helpful suggestions. I owe particular thanks to Professor Paul W. Pomeroy who first introduced me to the world of observational seismology and offered much guidance from the inception of the research to the writing of this dissertation.

Conversations with Drs. Ramesh Chander, Keith McCamy and James Brune also proved to be helpful. Drs. Sean Solomon and David Jackson provided me with preprints of their publications and Drs. Solomon and James Dorman kindly provided me with computed sets of Rayleigh wave partial derivatives. Fourier analysis was performed using a very efficient program written by Tim Swanson. I greatly appreciate the assistance of James Rust in processing some of the data. Finally, this research would not have been possible without the help and encouragement of my wife, Harriet.

During part of this research I was supported by a graduate traineeship of the National Science Foundation. This research was also supported in part by the Air Force Office of Scientific Research under contract F44620-69-C-0060 and by the Institute of Science and Technology of The University of Michigan.

TABLE OF CONTENTS

	Page
ACKNOWLEDGMENTS	ii
LIST OF TABLES	v
LIST OF ILLUSTRATIONS	vi
INTRODUCTION	1
BASIC THEORY IN MEASURING SEISMIC SURFACE WAVE ATTENUATION	3
DATA ANALYSIS PROCEDURE	6
DATA SELECTION	13
REGIONAL PATTERNS OF ATTENUATION OF RAYLEIGH WAVES ($10,000/Q_R$)	21
Eastern Canadian Shield	21
Western United States - Basin and Range	21
Western United States - Southern Rockies	23
Regional Patterns - A Summary and Some Speculations	26
INVERSION OF RAYLEIGH WAVE ATTENUATION DATA	32
MECHANISMS OF ATTENUATION	36
GENERAL COMMENTS ON FITTING INTRINSIC ATTENUATION MODELS TO THE OBSERVED RAYLEIGH WAVE ATTENUATION	40
MODELS OF INTRINSIC ATTENUATION FOR SELECTED REGIONS OF NORTH AMERICA	43
Eastern Canadian Shield	43
Basin and Range	51
Southern Rockies	51
INTERPRETATION OF INTRINSIC ATTENUATION MODELS	61
Crustal Zone of High Intrinsic Attenuation	61
Upper Mantle Zone of High Intrinsic Attenuation	65
SUGGESTIONS FOR FUTURE INVESTIGATIONS	70

Page

SUMMARY..... 72
REFERENCES..... 74
APPENDIX - FOURIER TRANSFORMS: FAST, DISCRETE, AND CONTINUOUS..... 82

LIST OF TABLES

Table		Page
1.	Parameters for the Events Used in $10,000/Q_R$ Measurements Where the Azimuthal Difference Between the Propagation Paths of Rayleigh Waves to the Station Pair was Less Than 1.0^o	18
2.	List of Seismograph Stations	19
3.	Frequency Independent Intrinsic Attenuation Model of the Eastern Canadian Shield (CANSD-1)	44
4.	Shear Velocities From CANSD and McEvilly's Central U.S. Canadian Shield Model (MUSCD)	44
5.	Frequency Independent Intrinsic Attenuation Model of the Eastern Canadian Shield (MUSCD-1)	47
6.	Intrinsic Attenuation Model of the Eastern Canadian Shield Assuming Localized General Relaxation Mechanisms (MUSCD-2)	47
7.	Frequency Independent Intrinsic Attenuation Model of the Basin and Range (BR-1)	53
8.	Intrinsic Attenuation Model of the Basin and Range Assuming Localized General Relaxation Mechanisms (BR-2)	53
9.	Frequency Independent Intrinsic Attenuation Model of the Southern Rockies (RMA-1)	57
10.	Intrinsic Attenuation Models of the Southern Rockies Assuming Localized General Relaxation Mechanisms (RMA-2, RMA-3)	57
11.	Frequency Independent Intrinsic Attenuation Model of the Southern Rockies (RMB-1)	59
12.	Intrinsic Attenuation Models of the Southern Rockies Assuming Localized General Relaxation Mechanisms (RMB-2, RMB-3)	59

LIST OF ILLUSTRATIONS

Figure		Page
1.	Variations in amplitude spectral density due to small changes in signal length.....	7
2.	Amplitude spectral densities of the different signal lengths shown in Figure 1a after they were smoothed by a moving average filter 0.01 Hz wide.....	8
3.	Effect of instrument response computed from different calibration pulses upon amplitude spectral density.....	10
4.	Effect of assuming the different amplitude spectral densities at Dugway, Utah shown in Figure 3 upon the computed Rayleigh wave attenuation ($10,000/Q_R$) for the path segment between Dugway (DUG) and Longmire, Washington (LON).....	11
5.	Rayleigh wave attenuation ($10,000/Q_R$) measurements for the path segment between Baker Lake, Northwest Territories (BLC) and Great Whale River, Quebec (GWC).....	15
6.	Rayleigh wave attenuation ($10,000/Q_R$) measurements for the path segment between Great Whale River, Quebec (GWC) and Seven Falls, Quebec (SFA).....	16
7.	Approximate path segments in North America over which Rayleigh wave attenuation ($10,000/Q_R$) was measured, and for which the azimuthal difference between great circle propagation paths from each epicenter to the stations at the ends of the path segment involved was less than 1.0^o.....	20
8.	Rayleigh wave attenuation ($10,000/Q_R$) measurements for path segments between Great Whale River, Quebec, and Schefferville, Quebec (GWC-SCH) and between Mould Bay, Northwest Territories and Schefferville,	

Figure		Page
	Quebec (MBC-SCH).....	22
9.	Rayleigh wave attenuation ($10,000/Q_R$) measurements for path segments in the Western United States (Basin and Range).....	24
10.	Rayleigh wave attenuation ($10,000/Q_R$) measurements for the path segment between Golden, Colorado (GOL) and Albuquerque, New Mexico (ALQ).....	25
11.	Qualitative models of regional patterns of relative peaks of Rayleigh wave attenuation ($10,000/Q_R$) for the Eastern Canadian Shield, the Southern Rockies (2 models) and the Basin and Range.....	27
12.	Regions of consistent Rayleigh wave attenuation patterns superimposed on the tectonic-heat flow map of Sclater and Francheteau (1970).....	28
13.	Theoretical $10,000/Q_R$ based on intrinsic attenuation ($10,000/Q_\beta$) model CANSD-1 compared with the Eastern Canadian Shield $10,000/Q_R$ pattern.....	45
14.	Theoretical $10,000/Q_R$ based on intrinsic attenuation ($10,000/Q_\beta$) models MUSCD-1 and MUSCD-2 compared with the Eastern Canadian Shield $10,000/Q_R$ pattern.....	48
15.	Theoretical $10,000/Q_R$ based on thermally activated intrinsic attenuation ($10,000/Q_\beta$) models compared with the Eastern Canadian Shield $10,000/Q_R$ pattern...	50
16.	Suggested shear wave velocity models of the Basin and Range compared with the Gutenberg Continental model.....	52
17.	Theoretical $10,000/Q_R$ based on intrinsic attenuation ($10,000/Q_\beta$) models BR-1 and BR-2 compared with the Basin and Range $10,000/Q_R$ pattern.....	54

Figure Page

18. Theoretical $10,000/Q_R$ based on intrinsic attenuation ($10,000/Q_\beta$) models RMA-1, RMA-2, and RMA-3 compared with the Southern Rockies $10,000/Q_R$ pattern (RMA)..... 58

19. Theoretical $10,000/Q_R$ based on intrinsic attenuation ($10,000/Q_\beta$) models RMB-1, RMB-2, and RMB-3 compared with the Southern Rockies $10,000/Q_R$ pattern (RMB)..... 60

20. Schematic frequency independent intrinsic attenuation ($10,000/Q_\beta$) models of the Eastern Canadian Shield, the Southern Rockies and the Basin and Range..... 62

INTRODUCTION

In this study regional models of the seismic attenuation properties of North America are proposed, based on measurements of the attenuation of Rayleigh waves in the 15 to 50 second period range. Over the years much seismological research has been concentrated on determining the elastic wave velocity distribution within the earth, i.e., the combination of purely elastic layers that will propagate seismic waves in the same travel times that have been measured in almost a century of observations. Anelastic or non-elastic properties have been considered by most investigators (e.g., Anderson et al., 1965) to have a negligible second order effect upon seismic wave velocities. These properties, however, have a first order effect upon seismic wave amplitudes; and after the elimination of geometric effects, the attenuation of a seismic wave is believed to be the most direct measure of the earth's anelasticity.

Most models of the attenuation properties of the earth (Knopoff, 1964; Anderson and Archambeau, 1964; Anderson et al., 1965; Teng, 1968; Tsai and Aki, 1969; Archambeau, Flinn, and Lambert, 1969) have assumed only radial variations. Lateral variations in seismic wave attenuation, observed in determining some of the above models have not appeared systematic and have been treated as scatter in the data. Attempts at defining lateral variations in attenuation properties have usually been limited to assigning a general crust and upper mantle attenuation property to each region or propagation path considered (e.g., Sutton et al., 1967; McGinley and Anderson, 1969; Molnar and Oliver, 1969; Solomon and Toksoz, 1970). This limitation is due in large part to the types of seismic phases analyzed, i.e., P, S, Pg, Lg, and Sn. Anderson et al. (1965) pointed out the advantages of analyzing longer period surface waves: less sensitivity to scattering and velocity reversals, accessibility to and lack of ambiguity of the path of

propagation, and the ability to relate the attenuation of different period surface waves to attenuation properties at different depths. Surface waves in the 15 to 50 second period range are long enough to retain these advantages, yet short enough to be sensitive to crustal and uppermost mantle properties.

The main purpose of this research has been to measure the attenuation of 15 to 50 second Rayleigh waves across different parts of North America, and invert these data to regional models of attenuation properties with depth. In addition it was hoped that correlation of attenuation properties with other known geophysical parameters such as seismic wave velocity and heat flow would increase our understanding of the attenuation mechanism or mechanisms involved. This knowledge is essential if seismic wave attenuation is to be related to earth structure, composition and dynamics. Regional models of attenuation properties with depth for the United States have also been suggested by Solomon (1971).

The following sections describe: basic theory in measuring seismic wave attenuation, data analysis and data selection procedures, regional values of attenuation of Rayleigh waves in the 15 to 50 second period range, the theory and assumptions involved in the inversion of Rayleigh wave attenuation data, regional models of attenuation properties with depth and their interpretation, and some suggestions with regard to future investigations.

BASIC THEORY IN MEASURING SEISMIC SURFACE WAVE ATTENUATION

It is possible to express (Brune, 1962; Sato, 1967) the surface disturbance corresponding to a given mode of a seismic surface wave as

$$u(r,t) \approx \frac{1}{2\pi} \int_0^{\infty} A(\omega) \frac{1}{\sqrt{\sin\theta}} e^{-ik^* r} \cos(\omega t - kr + \Phi(\omega))\, d\omega \qquad (1)$$

where the integral represents a summation of travelling sinusoidal components that attenuate with distance. In this equation

r = linear epicentral distance;

θ = angular epicentral distance;

t = propagation time;

$A(\omega)$ = amplitude density of the component of angular frequency ω at the source;

$\frac{1}{\sqrt{\sin\theta}}$ = geometrical spreading factor for a surface wave travelling over a spherical earth;

k = wave number;

$\Phi(\omega)$ = phase factor dependent upon the phase of the component at the source, and the number of times the surface wave has crossed a pole or antipode in travelling the distance r;

k^* = spatial attenuation coefficient expressing amplitude attenuation per unit of linear distance travelled.

Seismic wave attenuation may also be expressed as energy loss per cycle. Using terminology from electric circuit theory, we may define, after Knopoff (1964)

$$Q^{-1} = \Delta E / 2\pi E \qquad (2)$$

where Q^{-1} is the specific attenuation coefficient, ΔE is the elastic energy dissipated per cycle and E the maximum elastic energy stored

per cycle. Anderson (1968) has shown that for small attenuation

$$Q^{-1} = 2k^*/k \tag{3}$$

Brune (1962), Knopoff et al. (1964), and Anderson and Archambeau (1964) showed that for dispersed wave trains

$$Q^{-1} = \left(\frac{U}{c}\right) 2k^*/k \tag{4}$$

where U is the group velocity and c is the phase velocity. If equation (1) is thought of as the real part of a complex integral, k^* may be incorporated into $\bar{k}$, the complex wave number of the propagating wave, where $\bar{k} = k + ik^*$.

Q^{-1} may be computed for any sinusoidal component of a given mode of a surface wave travelling across a region of the earth. This is done by analyzing the seismograms at two stations that straddle this region and lie on the same great circle path as the epicenter. For a fixed r, equation (1) can be thought of as the real part of a complex Fourier integral and $A(\omega) \frac{1}{\sqrt{\sin\theta}} e^{-k^*r}$ is 2 $|\bar{A}(\omega)_r|$, or twice the modulus of the complex amplitude spectral density of this mode at angular frequency ω. Combining equations (1), (2), and (4) it is possible (Ben-Menahem, 1965; Tsai and Aki, 1969) to write

$$Q^{-1} = \ln\left(\frac{|\bar{A}(\omega)_{r_1}|}{|\bar{A}(\omega)_{r_2}|}\sqrt{\frac{\sin\theta_1}{\sin\theta_2}}\right) \Big/ \frac{\omega(r_2 - r_1)}{2U} \tag{5}$$

where $\bar{A}(\omega)_{r_1}$, $\bar{A}(\omega)_{r_2}$ = amplitude spectral densities for the angular frequency ω, computed from Fourier analysis of the surface wave traces at stations 1 and 2;

r_1, r_2, θ_1, and θ_2 = linear and angular epicentral distances at

stations 1 and 2.

In all the results discussed below Q^{-1} for Rayleigh waves, hereafter denoted as Q_R^{-1}, was determined using equation (5) and amplitude spectral densities computed from the vertical components of fundamental mode Rayleigh waves.

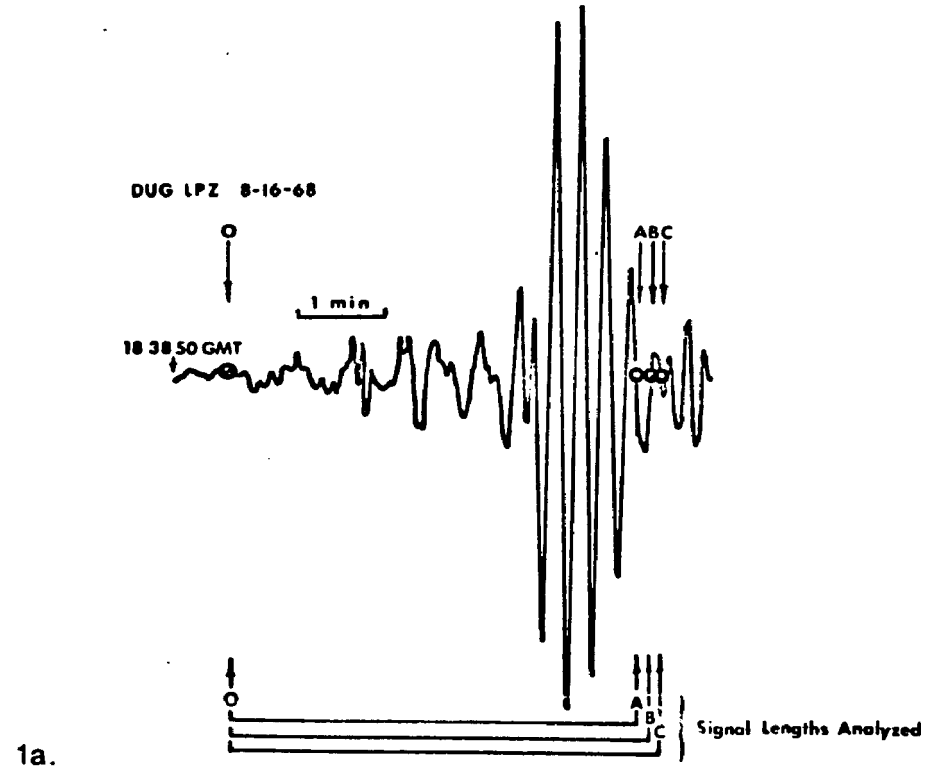
In most seismological studies measured attenuation appears as Q. Q^{-1} is considered to be a better term since it is the value used in all calculations and is directly proportional to the dissipation of energy (see equation (2)). In this study all Q^{-1} values were multiplied by 10,000 to avoid fractional values (see Jackson and Anderson (1970) for a recent tabulation of $10,000/Q$ for different types of seismic waves).

In the following sections the term attenuation is used interchangeably with $10,000/Q_R$. Subsequently, models of attenuation properties with depth will be proposed. These models are called intrinsic attenuation models and refer to the attenuation of compressional and shear waves ($10,000/Q_\alpha$ and $10,000/Q_\beta$) at different depths, rather than the resultant Rayleigh wave attenuation measured at the surface.

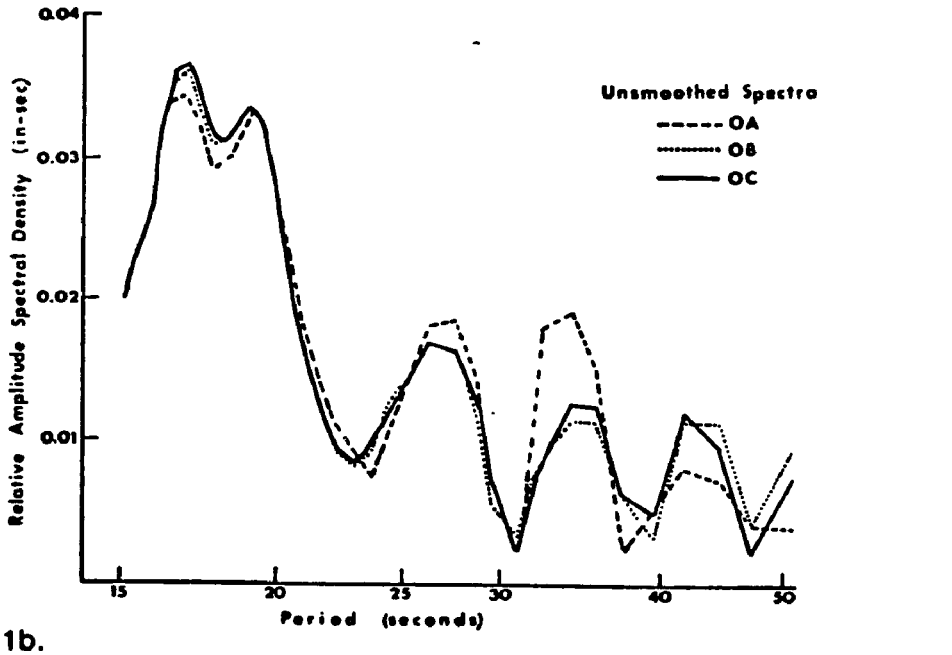
DATA ANALYSIS PROCEDURE

Seismograms selected for the determination of $10,000/Q_R$ over a given path were examined to determine what portion of the surface wave trace would be subjected to Fourier analysis. Ben-Menahem (1965) suggested using the same group velocity window for the signal pair involved in a single measurement. Group velocity is important since it is the velocity of propagation of the energy whose dissipation we are trying to measure. A laterally varying crust and upper mantle, however, imply laterally varying group velocities, especially at periods less than 30 seconds. It was decided, therefore, to use the same period windows for a signal pair, i.e., those parts of both surface wave trains that included resultant surface waves (energy arrivals) spanning a specified period range, usually 15 to 50 seconds. The limits of this period range were determined at one end by the presence of other seismic phases or higher Rayleigh wave modes and at the other end by the onset of irregular surface waves, attributed usually to the effects of scattering and reflections in the crust (Ewing, Jardetsky, and Press, 1957).

Since the location of the shorter period end of the surface wave train was not always clear, numerical experiments were conducted to determine what effects small changes in the length of an actual signal would have on the computed amplitude spectral density. These effects were not always negligible (Figure 1). However, it was observed that smoothing the resultant spectra minimized the differences between them (Figure 2). Tsai and Aki (1969) and Kanamori (1970) also applied spectral smoothing to the amplitude spectral densities of surface wave trains in order to minimize modulation phenomena in the frequency domain. This modulation was believed to be due to multi-path interference (Pilant and Knopoff, 1964). In this study the width of the spectral smoother (equally weighted, moving average filter) was 0.01 Hz. This width is the same as used by Tsai and Aki (1969). The actual number of



1a.



1b.

Figure 1. Variations in amplitude spectral density due to small changes in signal length: (a) vertical component of Rayleigh wave train from an earthquake near Oaxaca, Mexico (16.8°N, 97.7°W, origin time 18h 25m 55.1s GMT, Aug. 16, 1968) recorded at Dugway, Utah (DUG). The circles on the seismogram and the brackets below it indicate the extent of the signal Fourier analyzed; (b) amplitude spectral densities of the different signal lengths (unsmoothed).

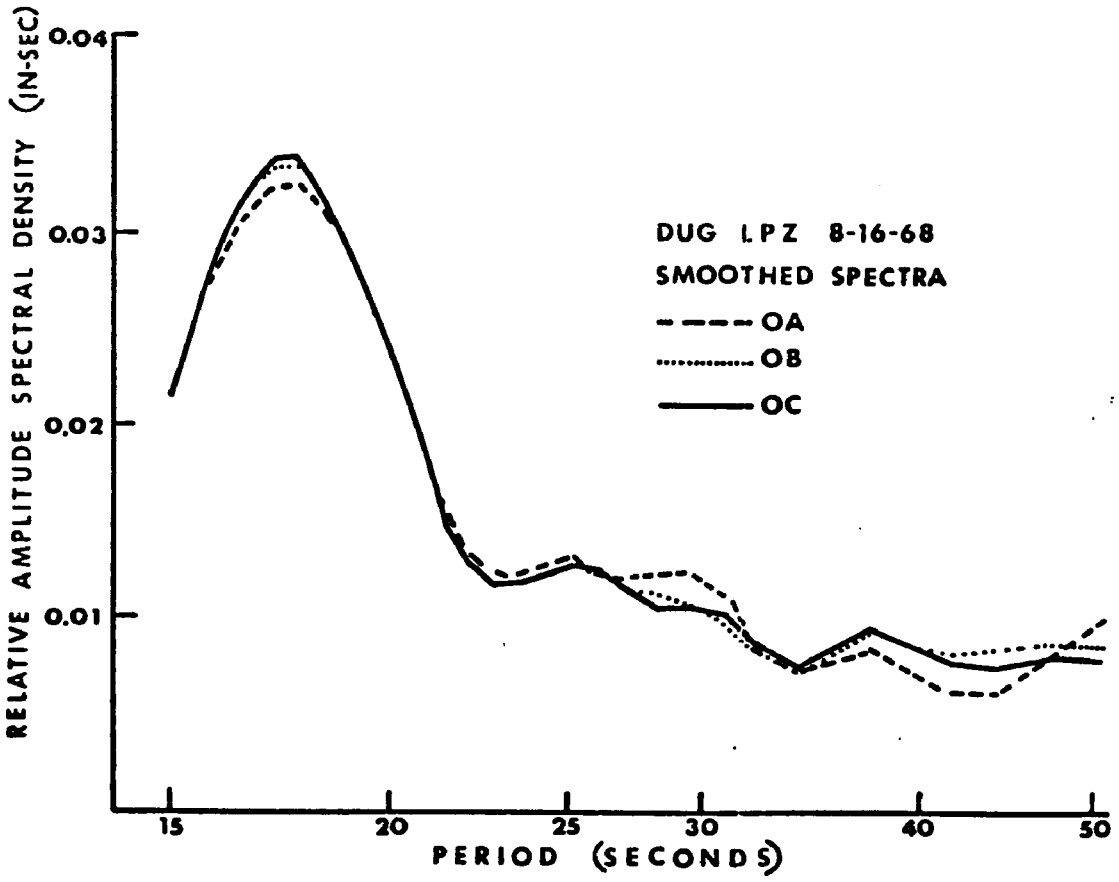


Figure 2. Amplitude spectral densities of the different signal lengths shown in Figure 1a after they were smoothed by a moving average filter 0.01 Hz wide.

points in the spectral smoother varied from 7 to 17, depending upon the time scale of the digitized seismogram.

The surface wave traces were digitized at intervals of 0.01 inch on the seismograms. These data were then interpolated to yield data points at time intervals of 1.17 seconds for most surface waves. Linear trends were removed and Fourier analysis was performed by means of the fast Fourier transform (see appendix). The amplitude spectra were then corrected for the instrument responses of the seismographs. The shapes of the instrument response curves were computed from the calibration pulses appearing on World Wide Standard Seismograph Network (WWSSN) seismograms or the instrument constants appearing on Canadian seismograms, using Brune's program for computation of instrumental response (Espinosa, Sutton and Miller, 1965). The curves for WWSSN seismographs were normalized to peak magnifications using Geotechnical Corporation (1961) formulas. Canadian seismograph instrument response curves were normalized to the peak magnifications noted on the seismograms.

The instrument response curves, particularly for periods greater than 30 seconds, were found to vary from station to station and time to time. Figure 3 shows smoothed amplitude spectral densities of the same Rayleigh wave train recorded at Dugway, Utah (DUG) from the event at Oaxaca, Mexico, described in Figure 1. DUG CAL-1 is the amplitude spectral density corrected for an instrument response calculated from the calibration pulse on the seismogram preceding the Rayleigh wave train, while DUG CAL-2 is the amplitude spectral density of the same signal corrected for an instrument response calculated from the calibration pulse on the seismogram following the Rayleigh wave train. The differences in these amplitude spectral densities led to markedly different values of $10,000/Q_R$ (Figure 4) when used to compute $10,000Q_R$ for the path segment between Dugway and Longmire, Washington (LON). The variability of computed instrument responses

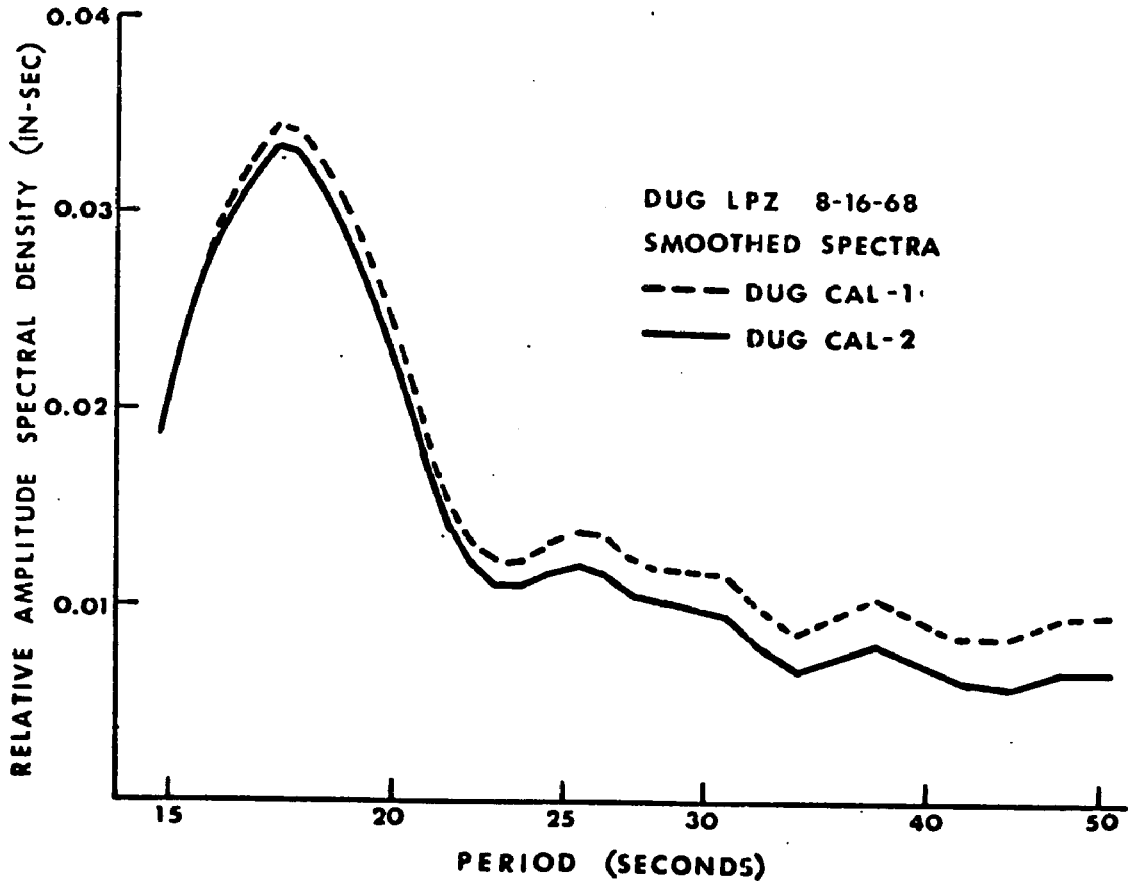


Figure 3. Effect of instrument response computed from different calibration pulses upon amplitude spectral density. DUG CAL-1 is the amplitude spectral density of the Rayleigh wave train from the same earthquake near Oaxaca, Mexico discussed in Figure 1, recorded at Dugway, Utah (DUG) and corrected for an instrument response computed from the calibration pulse preceeding the signal. DUG CAL-2, determined from the same Rayleigh wave train, was corrected for an instrument response computed from the calibration pulse following the signal.

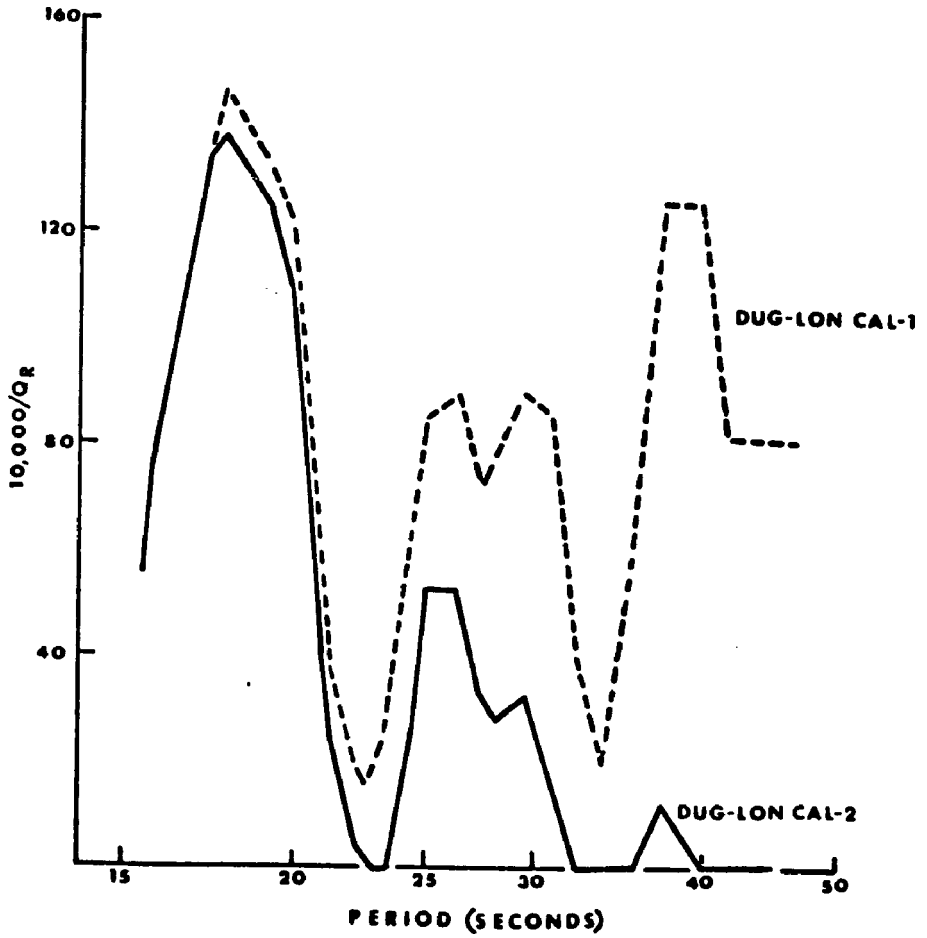


Figure 4. Effect of assuming the different amplitude spectral densities at Dugway, Utah shown in Figure 3 upon the computed Rayleigh wave attenuation ($10,000/Q_R$) for the path segment between Dugway (DUG) and Longmire, Washington (LON).

is believed to be a factor in causing the large observed variations in the values of $10,000/Q_R$ discussed below.

DATA SELECTION

Seismograms used in this study were taken from the World Wide Standard Seismograph Network for events in 1967 and 1968 and from the network maintained by the Seismological Service of Canada for events in 1967. Emphasis was placed on those earthquakes or explosions whose surface wave magnitude was greater than 5 and from whose epicenter great circle propagation paths crossed or came close to crossing pairs of seismograph stations in the Western United States or the Canadian Shield. Rayleigh waves from over 270 events were screened. Those Rayleigh wave trains that showed prominent beating, irregularity, or that were particularly weak were excluded. Amplitude spectral densities of the remaining Rayleigh wave trains (44) were analyzed and $10,000/Q_R$ computed using the procedure outlined in the preceding sections.

Group velocities used in equation (5) to compute $10,000/Q_R$ across the Canadian Shield were taken from the CANSD model of Brune and Dorman (1963). Group velocities used in computations of $10,000/Q_R$ across regions of the Western United States were determined from the particular seismograms involved. Since the propagation paths from the epicenters to the stations used often included large oceanic segments, these group velocities were compared to, and modified when necessary to better approximate the suggested continental Rayleigh wave dispersion curve of Oliver (1962) and the suggested basin-range Rayleigh wave dispersion curve of Brune (1969). Numerical experiments indicated, however, that any predictable error in the determination of group velocity had little effect upon the absolute value of computed $10,000/Q_R$ and no effect upon the pattern of relatively high and low attenuation within the period range analyzed.

The resultant $10,000/Q_R$ values were examined for regional consistency. Large variations in the absolute value of $10,000/Q_R$, often

exceeding an order of magnitude for a given period in different measurements across the same region, were observed. In addition, there were no consistent regional patterns of high or low relative attenuation confined to specific period ranges. These properties can be observed in Figure 5 which shows 3 separate determinations of $10,000/Q_R$ for the path segment between Baker Lake, Northwest Territories and Great Whale River, Quebec (BLC-GWC). Rayleigh waves from three separate events with epicenters near Hokkaido were used in these determinations. In this figure and in those following, ΔAZ is the angular separation in degrees of the azimuths from the epicenter to the two stations involved in the $10,000/Q_R$ computation. When $\Delta AZ = 0^o$ both stations and the epicenter lie on the same great circle. Also, a plotted value of $10,000/Q_R = 0$ for a particular period indicates either an increase or no decrease in the amplitudes of the Rayleigh waves at that period along the path of propagation.

Somewhat different conclusions may be drawn from Figure 6 which shows three separate determinations of $10,000/Q_R$ (from the same events used in Figure 5) for the path segment between Great Whale River and Seven Falls, Quebec (GWC-SFA). In this figure the variations in the absolute values of $10,000/Q_R$ for a given period are large but the relative peaks of attenuation, forming a definite pattern, fall in specific period ranges: 18 to 21 seconds, 29 to 32 seconds, and possibly rising attenuation at periods greater than 40 seconds. ΔAZ in all these determinations is less than 1^o. Although in the last two examples structural differences between the path segments cannot be ruled out, these and other observations suggested that restricting the $10,000/Q_R$ measurements to path segments where ΔAZ was small (less than 1^o) might improve the consistency of regional patterns of relative attenuation. This restriction means that the epicenter and both the stations involved in a single attenuation measurement would lie on a line which more closely approximated a great circle arc. This would reduce amplitude changes due to Rayleigh waves travelling over different

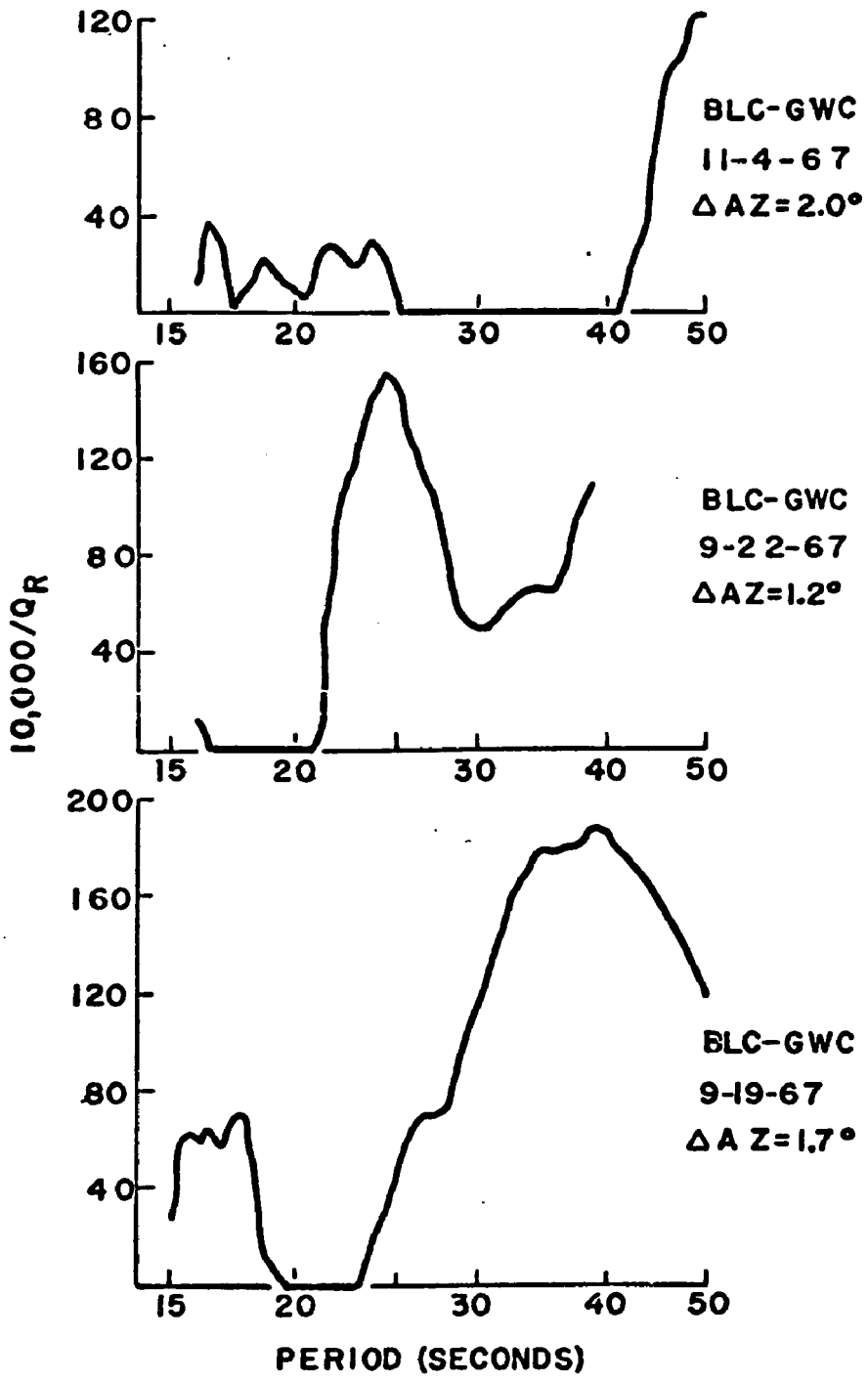


Figure 5. Rayleigh wave attenuation ($10,000/Q_R$) measurements for the path segment between Baker Lake, Northwest Territories (BLC) and Great Whale River, Quebec (GWC). ΔAZ is the azimuthal difference in degrees between great circle propagation paths from the epicenter to the stations.

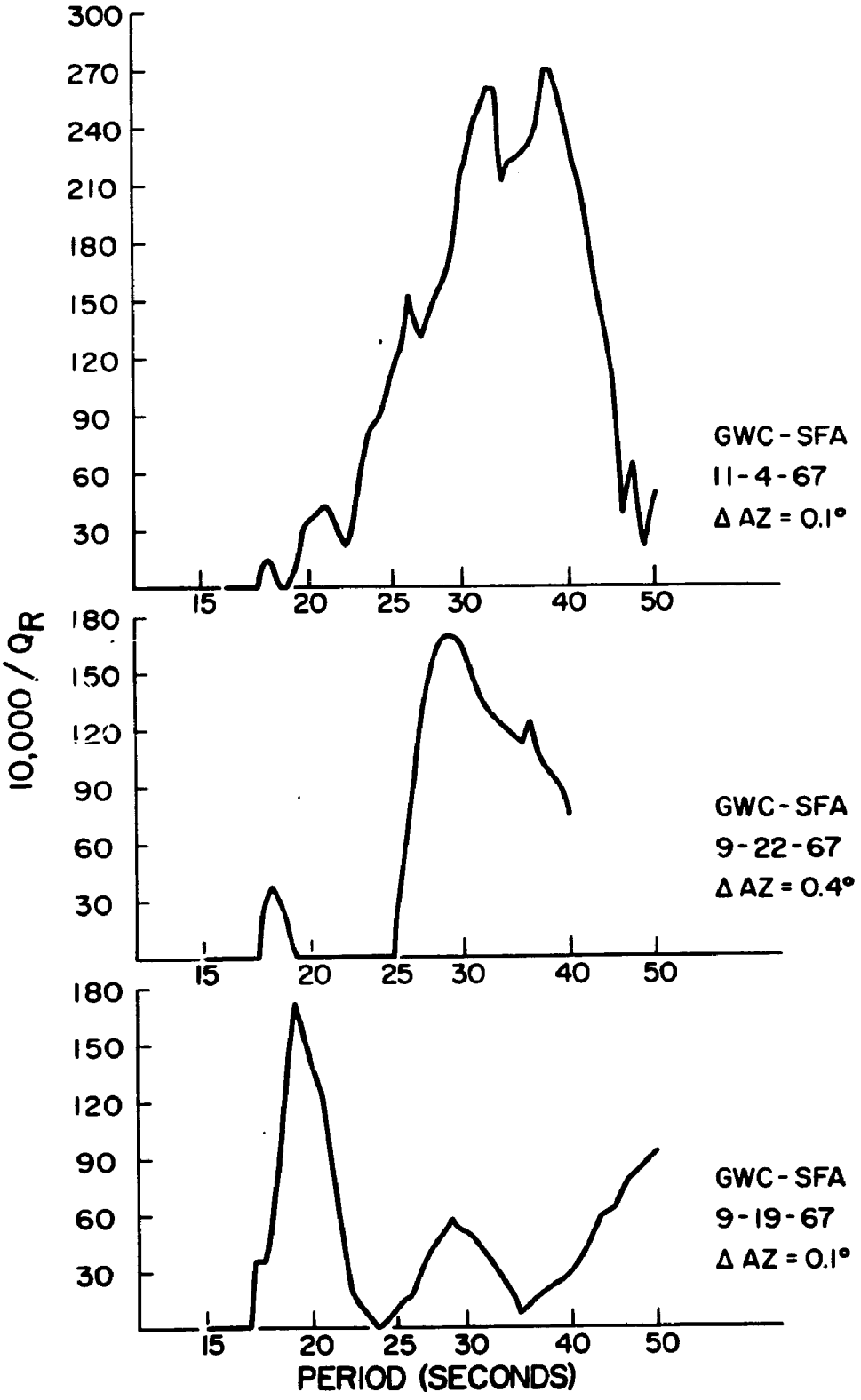


Figure 6. Rayleigh wave attenuation ($10,000/Q_R$) measurements for the path segment between Great Whale River, Quebec (GWC) and Seven Falls, Quebec (SFA).

structures before arriving at the path segment over which attenuation was to be measured, and to any intense azimuthal variations at the source.

Table 1 and Table 2 list the events and stations used in the $10,000/Q_R$ measurements for which Δ AZ was less than 1^o. Figure 7 shows the station pairs and approximate paths over which these measurements were made. The heavy solid lines represent path segments yielding patterns of attenuation consistent within their respective regions while the thin dashed lines show path segments over which patterns of attenuation were not consistent with others in the region. In general, large variations in the absolute value of $10,000/Q_R$ still remained; however, patterns of relative peaks of attenuation confined to specific period ranges were observed. These patterns were different for different regions of North America.

The $10,000/Q_R$ measurements for which Δ AZ was less than 1^o became the data set from which regional patterns of attenuation and resultant intrinsic attenuation models were determined.

TABLE 1

Parameters for the Events Used in $10,000/Q_R$ Measurements Where the Azimuthal Difference Between the Propagation Paths of Rayleigh Waves to the Station Pair Was Less Than 1.0^{o}.

Earthquake Parameters							Path Parameters		
Region	Latitude (Degrees)	Longitude (Degrees)	Date	Origin Time (GMT) Hr.	Min.	Sec.	Station	Epicentral Distance (km)	Azimuth to Station (Degrees)
Mexico-Quatamala Border	15.0 N	108.9 W	1-26-67	16	10	34.3	OTT	3730.8	22.0
							SCH	4956.0	21.2
Hokkaido	43.0 N	145.2 E	9-19-67	10	56	08.8	GWC	8396.3	23.7
							SFA	9425.7	23.8
							MNT	9490.4	26.3
							WES	9883.1	26.2
Kurile Islands	44.5 N	149.4 E	9-22-67	10	17	59.4	BLC	6679.6	27.2
							FCC	7178.2	31.1
							GWC	8102.6	26.0
							OTT	9114.2	30.3
							SFA	9131.1	26.4
Hokkaido	43.5 N	144.1 E	11-4-67	14	30	37.5	MBC	5532.0	18.2
							GWC	8380.9	23.2
							SCH	8738.8	17.6
							SFA	9410.3	23.1
Off coast of Oregon	44.2 N	128.9 W	12-28-67	22	11	33.9	GWC	3792.8	52.6
							SCH	4495.3	52.1
South of Panama	5.3 N	82.5 W	1-11-67	16	08	06.1	BOZ	5278.0	332.4
							FSJ	6608.8	333.1
Off coast of Central America	2.8 N	84.4 W	1-31-67	13	37	34.3	DUG	5030.5	329.1
							LON	6059.4	329.1
							VIC	6280.1	329.9
South of Kermadec Islands	33.9 S	179.6 W	10-18-67	22	06	23.5	BKS	9908.3	41.8
							BOZ	11136.3	41.4
Norwegian Sea	72.7 N	8.5 E	11-21-67	17	02	25.0	BOZ	6112.4	312.1
							GOL	6571.0	304.7
							DUG	6713.9	311.2
							ALQ	7102.9	303.9
							GSC	7333.8	313.0
Dominican Republic	18.8 N	69.6 W	5-2-68	5	29	38.2	ALQ	4041.1	303.8
							BKS	5491.3	304.1
South of Panama	5.6 N	82.6 W	6-15-68	7	08	48.1	DUG	4877.6	326.2
							LON	5904.0	327.0
Northern Easter Island Cordillera	4.4 S	104.9 W	10-22-68	7	45	56.1	TUC	4110.4	351.7
							DUG	5004.0	351.4
Svalbard	76.2 N	7.5 E	12-30-68	10	27	09.7	GOL	6328.2	301.9
							ALQ	6863.4	301.5

TABLE 2

List of Seismograph Stations

Station	Abbreviation	Latitude (Degrees N)	Longitude (Degrees W)
Albuquerque, New Mexico	ALQ	34.942	106.458
Baker Lake, Northwest Territories	BLC	64.316	96.017
Berkeley, California	BKS	37.876	122.235
Bozeman, Montana	BOZ	45.600	111.632
Dugway, Utah	DUG	40.195	112.813
Fort Churchill, Manitoba	FCC	58.763	94.087
Fort St. James, British Columbia	FSJ	54.433	124.250
Golden, Colorado	GOL	39.700	105.371
Goldstone, California	GSC	35.302	116.806
Great Whale River, Quebec	GWC	55.291	77.756
Longmire, Washington	LON	46.750	121.810
Montreal, Quebec	MNT	45.503	73.623
Mould Bay, Northwest Territories	MBC	76.242	119.360
Ottawa, Ontario	OTT	45.393	75.715
Schefferville, Quebec	SCH	54.816	66.784
Seven Falls, Quebec	SFA	47.123	70.828
Tucson, Arizona	TUC	32.309	110.782
Victoria, British Columbia	VIC	48.518	123.416
Weston, Massachusetts	WES	42.385	71.320

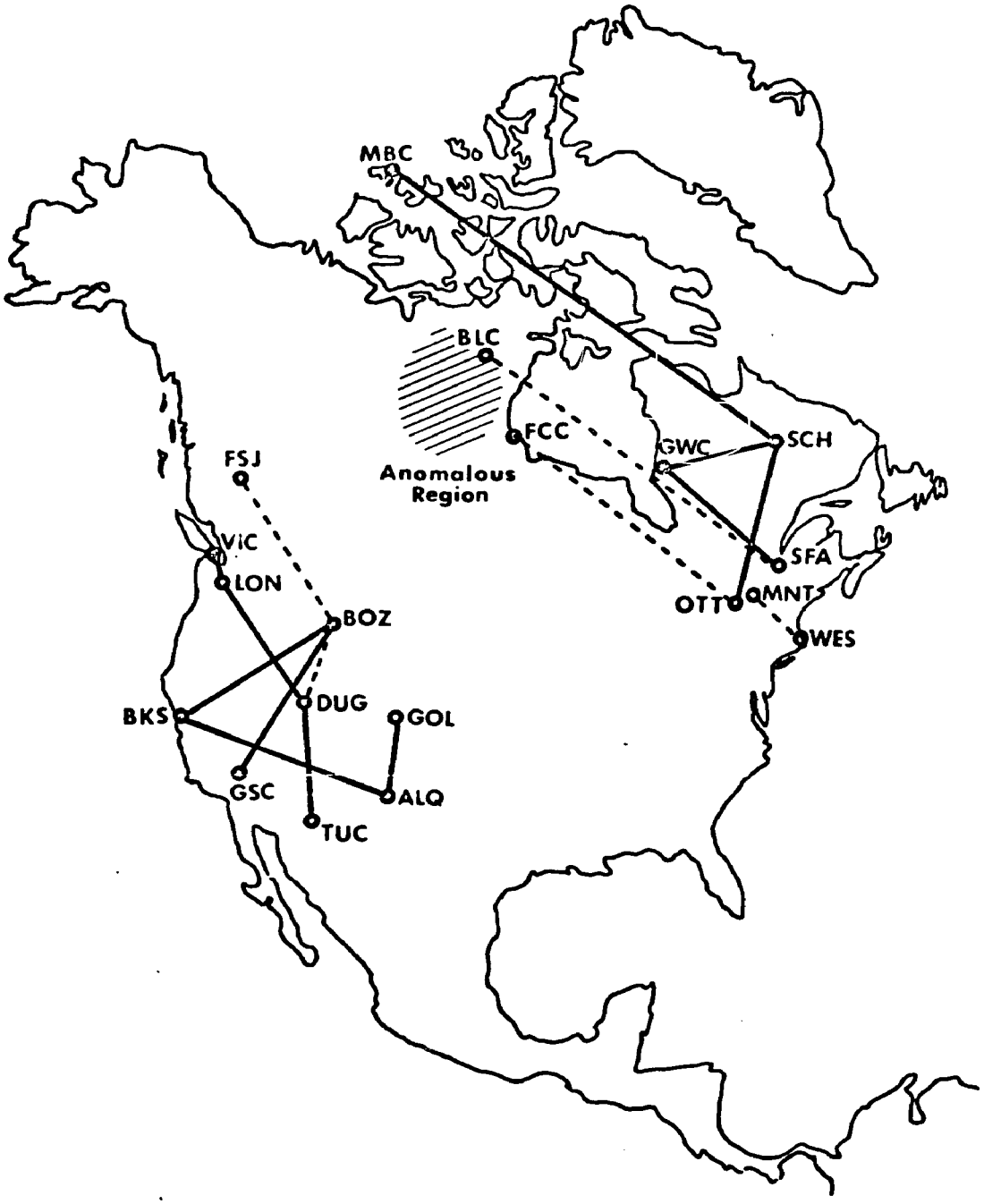


Figure 7. Approximate path segments in North America over which Rayleigh wave attenuation ($10,000/Q_R$) was measured and for which the azimuthal difference between great circle propagation paths from each epicenter to the stations at the ends of the path segment involved was less than 1.0°. Path segments shown as solid lines yielded $10,000/Q_R$ pattern consistent within the region while path segments shown as dashed lines did not. The anomalous region is the part of the Canadian Shield where most of the propagation paths yielding inconsistent $10,000/Q_R$ patterns cross (see text).

REGIONAL PATTERNS OF ATTENUATION OF RAYLEIGH WAVES ($10,000/Q_R$)

Eastern Canadian Shield

Measurements of $10,000/Q_R$ across the Eastern Canadian Shield gave repeated evidence of relative peaks of attenuation falling in the 18 to 21 and 29 to 32 second period ranges. This pattern was shown for the one path segment (GWC-SFA) shown in Figure 6. Figure 8 shows a similar pattern of relative attenuation measured along paths between Great Whale River and Schefferville, Quebec (GWC-SFA) and between Mould Bay, Northwest Territories (MBC) and Schefferville (MBC-SCH). Similarly, determination of $10,000/Q_R$ for the path segment between Ottawa, Ontario, and Schefferville (OTT-SCH) showed negative attenuation for the entire period range considered except for very small positive attenuation at 19 seconds ($10,000/Q_R < 1.0$) and 28 to 32 seconds ($10,000/Q_R < 5.0$). Attenuation measurements across or adjacent to the Canadian Shield not yielding values of $10,000/Q_R$ consistent with the general pattern were determined along path segments between Baker Lake, Northwest Territories and Seven Falls, Quebec (BLC-SFA), between Fort Churchill, Manitoba and Ottawa (FCC-OTT), and between Montreal, Quebec and Weston, Massachusetts (MNT-WES). These path segments are shown as thin dashed lines in Figure 7. Speculation as to the cause of this inconsistency is presented below. No definite pattern of attenuation for periods beyond 40 seconds could be observed aside from the possible increase in attenuation with period mentioned previously with regard to Figure 6.

Western United States - Basin and Range

Measurements of $10,000/Q_R$ between Tucson, Arizona and Dugway, Utah (TUC-DUG), Dugway and Longmire, Washington (DUG-LON), Berkeley, California, and Bozeman, Montana (BKS-BOZ), Bozeman and Goldstone, California (BOZ-GSC), and Albuquerque, New

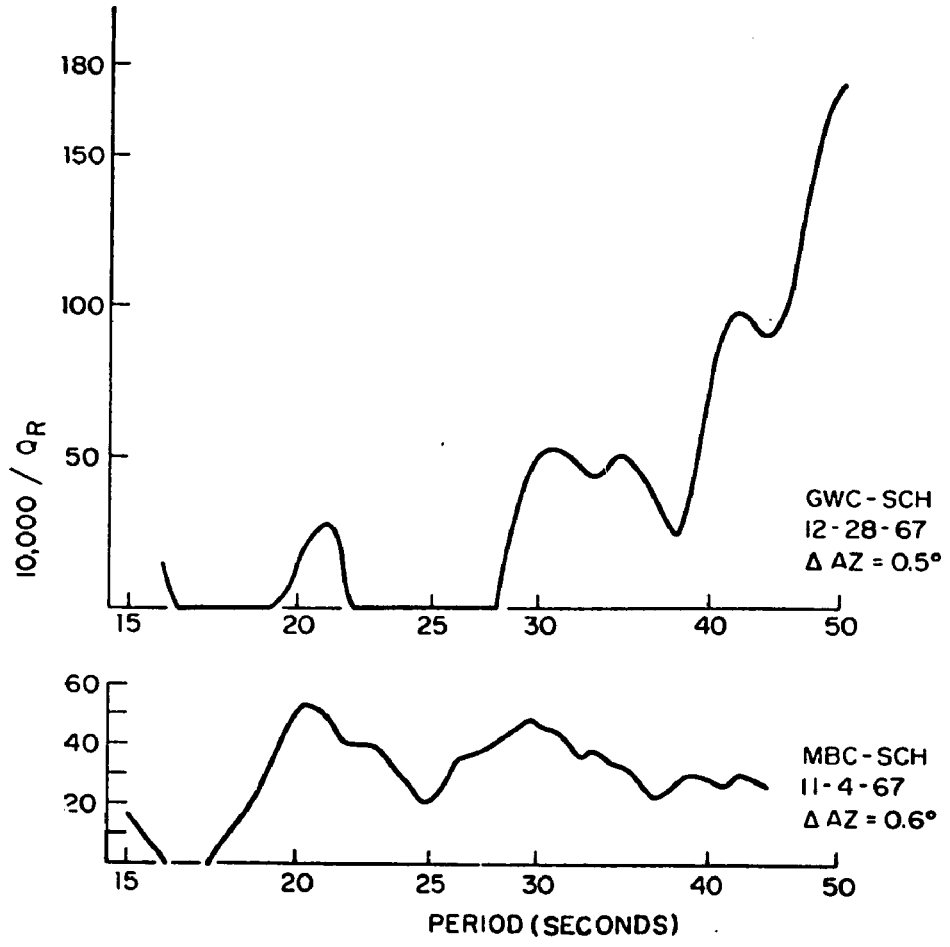


Figure 8. Rayleigh wave attenuation ($10,000/Q_R$) measurements for path segments between Great Whale River, Quebec and Schefferville, Quebec (GWC-SCH) and between Mould Bay, Northwest Territories and Schefferville, Quebec (MBC-SCH).

Mexico, and Berkeley (ALQ-BKS) exhibit a pattern of higher attenuation at 15 seconds and a relative peak of attenuation between 19 and 24 seconds. At periods greater than 35 seconds the pattern fluctuates although attenuation increasing with period is sometimes indicated. The region defined by these path segments in Figure 7 covers the Basin and Range province although segments of other provinces are included. The individual $10,000/Q_R$ determinations are shown in Figure 9.

The relatively greater variation in the positioning of peaks of attenuation when compared with the Canadian Shield measurements shown in Figures 6 and 8 is most likely due to the greater structural complexity of the Western United States. In addition, $10,000/Q_R$ for the BKS-BOZ segment in Figure 9 was measured using Rayleigh waves from an event whose epicenter was in the Kermadec region. McGarr (1969) documented large variations in the Rayleigh wave amplitudes of events in this region recorded at different stations in the United States. He attributed this to variations in the velocity structure near the epicentral region. Attenuation measurements in Western United States (and Southwestern Canada) yielding values of $10,000/Q_R$ inconsistent with the general pattern mentioned above were determined along path segments between Bozeman and Dugway (BOZ-DUG) and between Bozeman and Fort St. James, British Columbia (BOZ-FSJ). These path segments are shown as thin dashed lines in Figure 7.

Western United States - Southern Rockies

Two measurements of $10,000/Q_R$ between Golden, Colorado, and Albuquerque, New Mexico (GOL-ALQ) are shown in Figure 10. It is difficult to determine a pattern of attenuation for this region (the Southern Rockies) with these measurements alone. It is assumed that a peak of attenuation exists between 15 and 16 seconds even though it occurs in only one of the measurements (11-21-67). In the other measurement (12-30-68) fundamental mode Rayleigh waves were not observed at periods less than 16 seconds. At longer periods, either the existence of

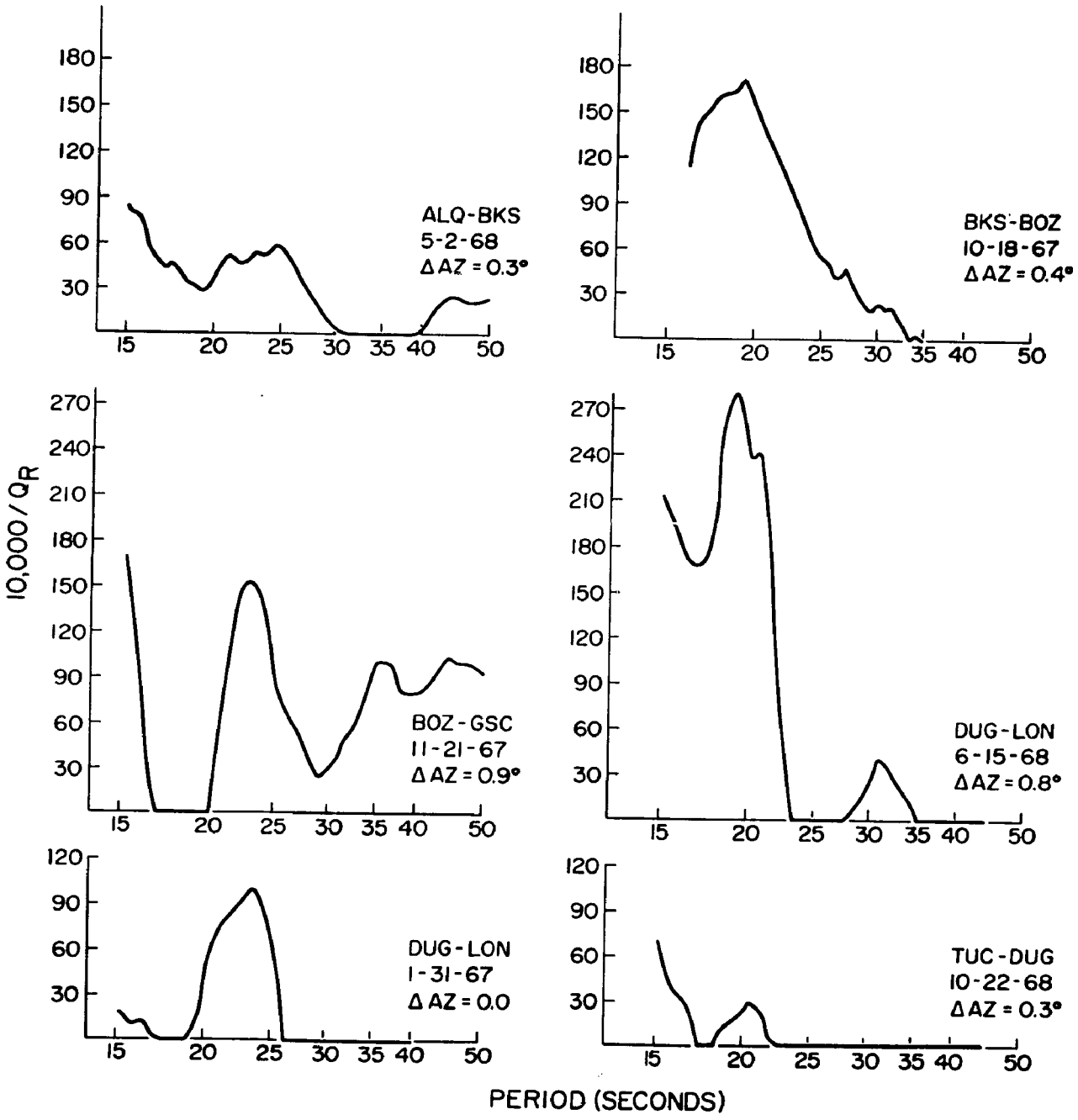


Figure 9. Rayleigh wave attenuation ($10{,}000/Q_R$) measurements for path segments in the Western United States (Basin and Range).

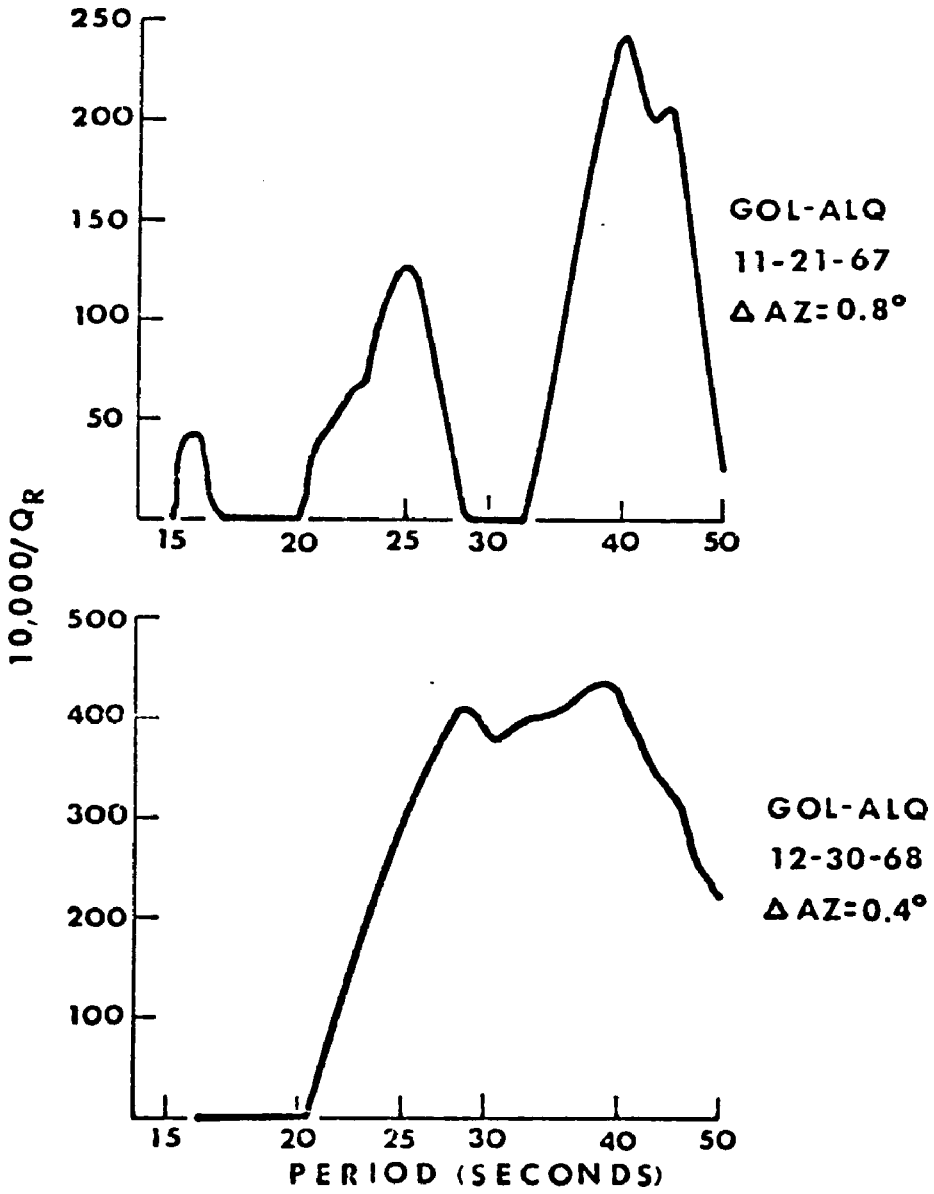


Figure 10. Rayleigh wave attenuation ($10,000/Q_R$) measurements for the path segment between Golden, Colorado (GOL) and Albuquerque, New Mexico (ALQ).

peaks of attenuation between 25 and 28 seconds and between 39 and 40 seconds or the existence of one broad peak of attenuation between 31 and 35 seconds was considered possible. Both these suggested patterns were used in the interpretation and inversion discussed below.

$10,000/Q_R$ was also measured for a path segment between Longmire, Washington and Victoria, British Columbia (LON-VIC). Although it did exhibit peaks of attenuation similar to those observed for the Western United States, particularly the Southern Rockies, only one event was used, and the absolute value of $10,000/Q_R$ measured was so high (e.g., $10,000/Q_R$ at 17 seconds was 878) that it was not considered as a separate pattern. The high attenuation may be a result of faulty determination of the instrumental constants or a sharp structural contrast between the North American mainland and Vancouver Island (Wetmiller, 1970).

Regional Patterns - A Summary and Some Speculations

Figure 11 shows qualitative models of the regional patterns of relative peaks of attenuation discussed in the previous sections. No quantitative estimate is given for attenuation ($10,000/Q_R$) at any period. For each model the period ranges within which the relative peaks of attenuation were confined are indicated by the position and width of the peaks shown. The sloping sides of these peaks represent the addition of half-widths (0.005 Hz) of the spectral smoother used on the amplitude spectral densities. Rising attenuation at long periods suggested by only some of the measurements is shown as a dotted line in the Eastern Canadian Shield and Basin and Range models.

The regions crossed by the path segments consistent for each attenuation model are shown in Figure 12 superimposed on a tectonic map of North America (Sclater and Francheteau, 1970). This map, based on the tectonic map of King (1969) was modified by Sclater and Francheteau to reflect regional heat flow properties. Of particular importance is the United States portion of the Cenozoic Basin and Range

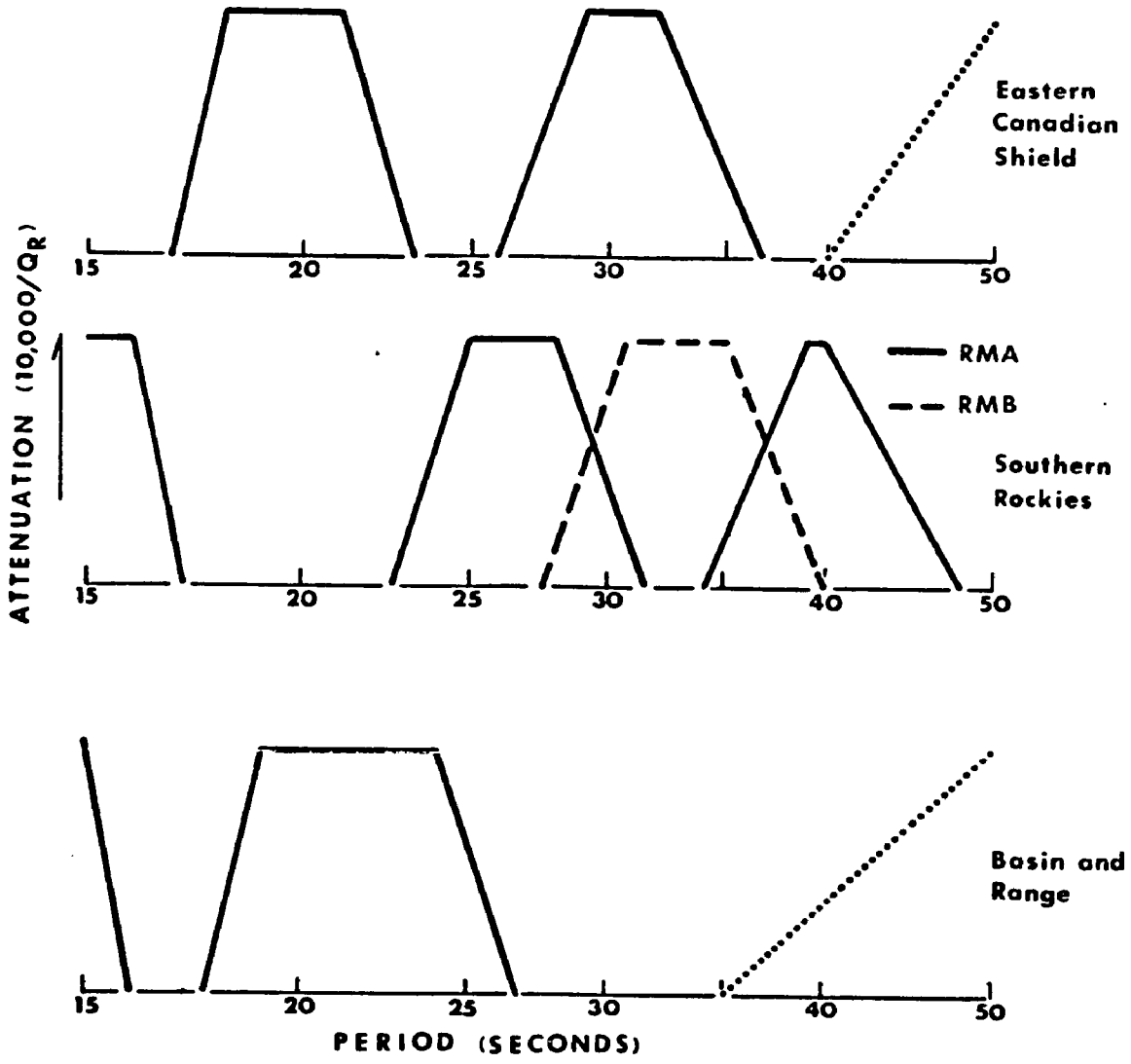


Figure 11. Qualitative models of regional patterns of relative peaks of Rayleigh wave attenuation ($10,000/Q_R$) for the Eastern Canadian Shield, the Southern Rockies (2 models) and the Basin and Range. Possible rising attenuation at long periods is shown as a dotted line.

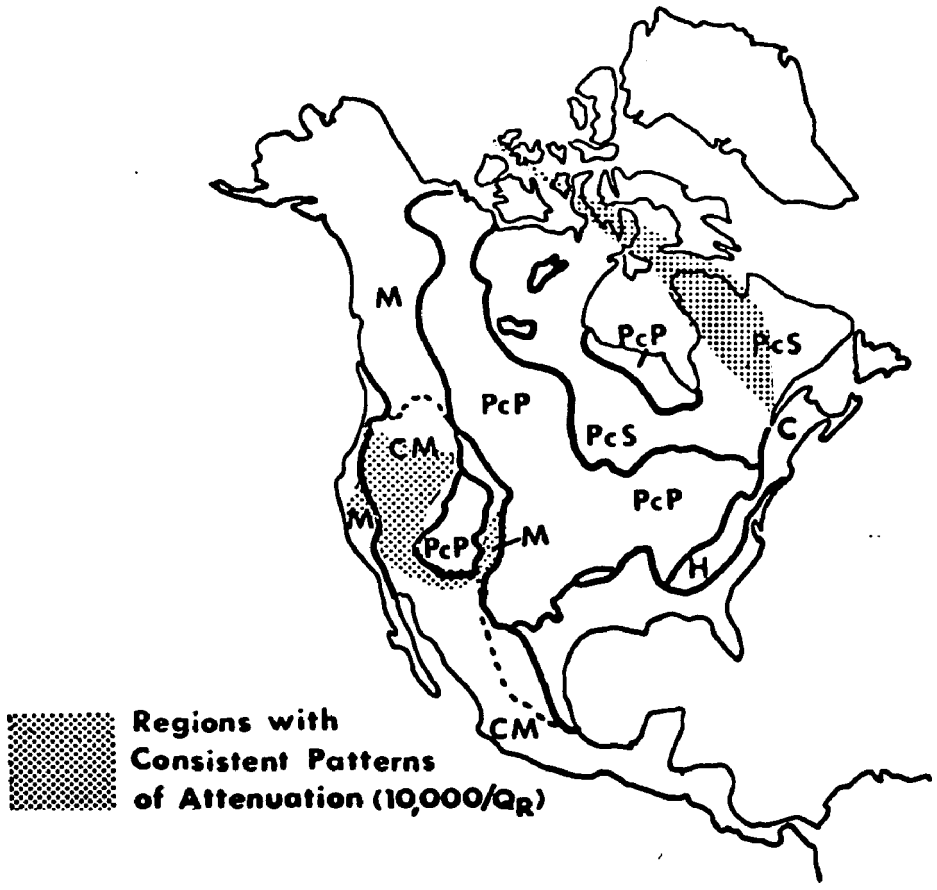


Figure 12. Regions of consistent Rayleigh wave attenuation patterns superimposed on the tectonic-heat flow map of Sclater and Francheteau (1970). In this classification CM is Cenozoic Basin and Range provinces, M is Mesozoic orogenic belts, H is Hercynian orogenic belts, C is Caledonian orogenic belts, PcP is Precambrian Platforms and PcS is Precambrian Shields.

provinces (CM). This section includes the classical Basin and Range, Columbia Plateau, and Northern Rocky Mountains. Blackwell (1969) also called this the Cordilleran Thermal Anomaly Zone, since there are high heat flow measurements throughout the whole province. This region coincides almost completely with the region associated with the Basin and Range attenuation model of Figure 11. Similarly, the regions associated with the Southern Rockies and Eastern Canadian Shield attenuation models of Figure 11 coincide with portions of the Mesozoic orogenic belts (M) and Precambrian Shields (PcS) of Figure 12. The mean heat flow for each of these provinces in North America is 2.2 μ cal cm^{-2} sec^{-1} for Cenozoic Basin and Range provinces, 1.6 μ cal cm^{-2} sec^{-1} for Mesozoic orogenic belts, and 0.9 μ cal cm^{-2} sec^{-1} for Precambrian Shields (Sclater and Francheteau, 1970). If the peaks in each model shown in Figure 11 can be related, then there is a shift of high attenuation to longer periods as the transition from the young, high heat flow Basin and Range to the old, low heat flow Canadian Shield is made. Whether attenuation is directly related to heat flow or both are connected by other parameters cannot be determined from this study.

Speculation as to why the path segments shown as dashed lines in Figure 7 yielded attenuation patterns inconsistent with others in their regions rests upon the postulated lateral refraction of surface waves. Lateral refraction has been suggested by many investigators as an explanation of observed variations in surface wave amplitudes. McGarr (1969) suggested that an anomalous velocity structure beneath Hawaii acts as a lens, refracting Rayleigh waves so that they focus in certain regions, causing higher amplitudes to be recorded there. He also suggested that oceanic trenches refract Rayleigh waves with a similar effect. Capon (1970), analyzing Rayleigh wave arrivals at the large aperture seismic array (LASA) in Montana believed that delayed energy arrivals at different periods were due to a differential refraction of the Rayleigh waves at the continental margin. Savarensky et al. (1969) divided the

North Atlantic into 3 crustal models and computed the resultant lateral refraction for 6 and 20 second Rayleigh waves propagating across this region. They pointed out zones of ray condensation and rarefaction where the different period Rayleigh waves would be relatively stronger or weaker.

Based on the discussion below it is suggested that there exist deep structural or velocity contrasts beneath the Northwestern Canadian Shield that are sufficient to cause differential refraction of Rayleigh waves propagating along paths that almost coincide (i.e., Δ AZ $< 1^{o}$). $10,000/Q_R$ computed from amplitudes measured at stations along these propagation paths should then vary considerably and not reflect any general $10,000/Q_R$ pattern determined from Rayleigh waves that passed near to but not through the region of deep contrast. The Rayleigh waves used to determine $10,000/Q_R$ along the MNT-WES, FCC-OTT, and BOZ-DUG path segments, and those arriving at BLC (of the BLC-SFA path segment) all passed through the western part of the Churchill province of the Canadian Shield shown as an anomalous region in Figure 7. Aside from BOZ-GSC all path segments in Figure 7 that yielded attenuation patterns consistent with the regional models shown in Figure 11 were associated with Rayleigh wave propagation paths passing to the northeast or south of this region.

Significant differences in the crustal and upper mantle velocity structures between different provinces of the Canadian Shield have been suggested independently by Weichert (1968) and Wickens and Pec (1968). Similarly, analysis of seismic refraction results from the Hudson Bay and Early Rise Experiments (Hunter and Mereu, 1967; Mereu and Hunter, 1969) show a markedly thicker crust (40 to 50 kilometers) beneath the western Churchill province north of the Nelson River and west of the center of Hudson Bay. Although the time term method used in this analysis has been subjected to criticism when it is used to determine sharply sloping refractor depths (Reiter, 1970), a relatively thicker crust in the western Churchill province cannot be disputed.

However, any hypothesis regarding the anomalous structure of this part of the Canadian Shield must await the compilation of more data.

Presently, the only suggestion that can be offered regarding the regionally inconsistent attenuation pattern determined along the BOZ-FSJ path segment is that the anomalous pattern is related to this path segment crossing the Rocky Mountain Trench.

Additional measurements by this writer of attenuation along typical oceanic paths in the Central Pacific have to date not yielded any apparent pattern of attenuation. The lack of consistency for the paths studied is clear although oceanic structure is generally less complex than continental structure. This absence of pattern is due perhaps to the sparsely located seismograph stations in the area being unable to record Rayleigh waves that were not laterally refracted by oceanic trenches and ridges.

INVERSION OF RAYLEIGH WAVE ATTENUATION DATA

The attenuation of sinusoidal components of Rayleigh waves can be related to intrinsic attenuation (attenuation of compressional and shear waves) as a function of depth by means of a theory presented by Anderson and Archambeau (1964) and Anderson, Ben-Menahem, and Archambeau (1965). Use is made of the dispersion relation for a layered medium $c(\omega) = \omega/k = f(h_n, \alpha_n, \beta_n, \rho_n)$ where $c(\omega)$ is the Rayleigh wave phase velocity at angular frequency ω, k is the wave number and h_n, α_n, β_n, and ρ_n are the thickness, compressional and shear wave velocities, and density of the nth layer.

Attenuation is introduced by expressing phase velocity as a complex quantity $\bar{c} = c - ic^*$, related to a complex wave number $\bar{k} = k + ik^*$. $\bar{k}$ is itself due to complex compressional and shear wave velocities $\bar{\alpha}_n = \alpha_n - i\alpha_n^*$ and $\bar{\beta}_n = \beta_n - i\beta_n^*$ in the different layers, while ω, h_n and ρ_n remain real. The dispersion relation is expanded into a Taylor Series treating the imaginary components of the layer velocities α_n^*, and β_n^* as increments to the real or propagating velocities α_n, and β_n. Under the assumption that α_n^* and β_n^* are small, k^* may be written as

$$k^* = \frac{k^2}{\omega} \sum_{n=1}^{N} \left[\alpha_n^* \left(\frac{\partial c}{\partial \alpha_n} \right)_{k,\beta,\rho} + \beta_n^* \left(\frac{\partial c}{\partial \beta_n} \right)_{k,\alpha,\rho} \right] \qquad (6)$$

where N is the number of layers in the waveguide. If $k_{\alpha_n}^*$ and $k_{\beta_n}^*$ are the complex body wave numbers associated with the nth layer complex velocities defined above, equation (3) may be extended to

$$Q_{\alpha_n}^{-1} = \frac{2k\alpha_n^*}{k\alpha_n} = \frac{2\alpha_n^*}{\alpha_n}$$

and

$$Q_{\beta_n}^{-1} = \frac{2k_{\beta n}^*}{k_{\beta n}} = \frac{2\beta_n^*}{\beta_n} \tag{7}$$

where $Q_{\alpha_n}^{-1}$ and $Q_{\beta_n}^{-1}$ are the intrinsic compressional and shear wave attenuation factors of the nth layer. Using equations (6) and (7) and letting k and k* in equation (4) refer to the real and imaginary parts of the complex wave number of the Rayleigh wave component, we may write

$$Q_R^{-1} = \sum_{n=1}^{N} \left[\left(\frac{\alpha_n}{c} \frac{\partial c}{\partial \alpha_n} \right)_{k,\beta,\rho} Q_{\alpha_n}^{-1} + \left(\frac{\beta_n}{c} \frac{\partial c}{\partial \beta_n} \right)_{k,\alpha,\rho} Q_{\beta_n}^{-1} \right] \tag{8}$$

where Q_R^{-1} is the specific attenuation of that component. The assumptions involved in arriving at equation (8) are worth reiterating:

1. The medium, i.e., the earth, is a layered waveguide.

2. Attenuation is a result of non-elastic properties that can be described by means of complex body wave velocities. Attenuation due in whole or part to imperfect inertia and describable by a complex density is not considered. Complex body wave velocities may be written in terms of complex elastic moduli and real densities:

$$(\bar{\alpha}_n)^2 = \left[\bar{K}_n + (4/3)\bar{\mu}_n\right]/\rho_n \qquad (\bar{\beta}_n)^2 = \bar{\mu}_n/\rho_n \tag{9}$$

where the complex incompressibility $\bar{K}_n = K_n - iK_n^*$ and the complex rigidity $\bar{\mu}_n = \mu_n - i\mu_n^*$. The intrinsic attenuation of a specific layer

may then be written as

$$Q\alpha_n^{-1} = [K_n^* + (4/3)\mu_n^*] / [K_n + (4/3)\mu_n]$$

and

$$Q\beta_n^{-1} = \mu_n^* / \mu_n \qquad (10)$$

3. Intrinsic attenuation is small, i.e., $Q\alpha_n^{-1}$, $Q\beta_n^{-1} \ll 1.0$.

If an anelastic earth model is considered to be a perturbation of an assumed elastic earth model, $\frac{\partial c}{\partial \alpha_n}$ and $\frac{\partial c}{\partial \beta_n}$ can be computed based upon the elastic earth model and along with the assumed body wave and phase velocities be used in equation (8). Some set of $Q\alpha_n^{-1}$ and $Q\beta_n^{-1}$ can then be found that will yield Q_R^{-1} that best approximates the observed Q_R^{-1}. In this procedure there are two unknowns for each layer, $Q\alpha_n^{-1}$ and $Q\beta_n^{-1}$, or K_n^* and μ_n^*. Using Rayleigh wave observations alone, it is not possible to separate these quantities. Most investigators of both Love and Rayleigh wave attenuation (e.g., Anderson, Ben-Menahem and Archambeau, 1965; Tsai and Aki, 1969) have neglected losses or attenuation due to imperfect incompressibility (K*) and assumed the earth to be a Poisson solid when relating $Q\alpha_n^{-1}$ to $Q\beta_n^{-1}$. These assumptions yield $Q\alpha_n^{-1} = (4/9)\, Q\beta_n^{-1}$ and in general agree with their observations. Since the Rayleigh wave partial derivatives used in equation (8) usually assign a much greater weight to $Q\beta_n^{-1}$, small deviations from the above assumptions will not have an appreciable effect on any computed Q_R^{-1}. Under these assumptions Q_R^{-1} may be expressed as a weighted function of $Q\beta_n^{-1}$ alone:

$$Q_R^{-1} = \sum_{n=1}^{N} \left[\frac{4}{9} \left(\frac{\alpha_n}{c} \frac{\partial c}{\partial \alpha_n} \right)_{k,\beta,\rho} + \left(\frac{\beta_n}{c} \frac{\partial c}{\partial \beta_n} \right)_{k,\alpha,\rho} \right] Q_{\beta_n}^{-1} \qquad (11)$$

Equation (11), multiplied by a constant factor of 10,000, was used in determining the regional models of intrinsic attenuation ($10,000/Q_\beta$) discussed below.

MECHANISMS OF ATTENUATION

It was pointed out above that the only assumption made regarding the actual mechanism of seismic wave attenuation was that it was caused by a small departure from pure elasticity mathematically describable by means of a complex elastic modulus. An important question for the observational seismologist in determining and using attenuation measures (e.g., Q_β^{-1}) is whether they are independent of or dependent upon frequency in the period range of observed seismic waves. This question cannot be answered by surface wave observations alone. Because of the very nature of surface waves, surface wave attenuation (e.g., Q_R^{-1}) would exhibit frequency dependence even though the intrinsic attenuation properties (Q_α^{-1}, Q_β^{-1}) of the earth were frequency independent and varied only with depth. It would be very difficult to separate this built-in frequency dependence from that due to the frequency dependence of the intrinsic attenuation properties themselves.

Theoretical and laboratory investigations into the nature of the attenuation mechanism have yielded a wealth of literature in recent years (see Knopoff, 1964; Anderson, 1967; and Jackson and Anderson, 1970, for reviews of these investigations). However, definition of the actual mechanism or mechanisms involved has yet to be accomplished. One of the more basic contradictions is the fact that investigations of elastic wave propagation under laboratory conditions yield a Q^{-1} essentially independent of frequency (Attewell and Ramana, 1966), while most of the proposed attenuation mechanisms require frequency dependence (Jackson and Anderson, 1970).

A large group of these frequency dependent mechanisms may be classified as relaxation mechanisms. Jackson and Anderson (1970) have defined relaxation taking place '... when stress causes a change in the condition of the solid that is reversed upon reversal of the stress (e.g., thermoelastic heating, phase changes, short excursions of defects)...

This process acts to relieve the instantaneous stress, causing linear, frequency dependent, internal friction (Q^{-1}).' A generalized relaxation mechanism can be understood by examining the standard linear solid of Zener (1948). In this mechanical model wave motion, i.e., periodic stress and strain are related by means of a complex elastic modulus:

$$\bar{M} = M_R\left(\frac{1+\omega^2\tau_\sigma\tau_\epsilon}{1+\omega^2\tau_\epsilon^2}\right) + i\,\frac{M_R\,\omega(\tau_\sigma-\tau_\epsilon)}{1+\omega^2\tau_\epsilon^2} \tag{12}$$

where M_R is the relaxed modulus, τ_ϵ the relaxation time of stress under constant strain, τ_σ the relaxation time of strain under constant stress and ω the angular frequency of applied stress and resultant strain. Relaxation time is defined as the time in which it takes stress or strain to fall to 1/e of its initial value. In the standard linear solid τ_σ is greater than τ_ϵ , and M_U or the unrelaxed modulus is related to M_R by

$$M_U = \left(\frac{\tau_\sigma}{\tau_\epsilon}\right)M_R \tag{13}$$

M_U is the effective real modulus of the system for relatively high frequency stress and M_R the effective real modulus for relatively low frequency stress.

Attenuation or internal friction in this system is equal to the tangent of the phase lag angle between stress and strain, i.e.,

$$Q^{-1} = \tan\delta = \left(\frac{M_U-M_R}{\sqrt{M_U M_R}}\right)\frac{\omega\bar{\tau}}{1+\omega^2\bar{\tau}^2} = \Delta_o\frac{\omega\bar{\tau}}{1+\omega^2\bar{\tau}^2} \tag{14}$$

where $\bar{\tau} = \sqrt{\tau_\epsilon\tau_\sigma}$, and Δ_o is the modulus defect or relaxation strength. For high frequency ($\omega >> \frac{1}{\bar{\tau}}$), $Q^{-1} \approx \Delta_o/\omega\bar{\tau}$; for low frequency ($\omega << \frac{1}{\bar{\tau}}$), $Q^{-1} \approx \Delta_o\,\omega\bar{\tau}$. Q^{-1} is maximum when $\omega = 1/\bar{\tau}$. By defining Δ_o and $\bar{\tau}$ we then define a Q^{-1} that is very pronounced in a certain period range while in others it is very small. In modeling

intrinsic attenuation, this property allows us to enhance or mask the effect of the weighting function shown in brackets in equation (11). Changing $\bar{\tau}$ for a particular layer may change the effect the intrinsic attenuation of that layer has upon $10,000/Q_R$ at different periods. Alternately, similar values of $10,000/Q_R$ may be brought about by different models of intrinsic attenuation by means of changes in $\bar{\tau}$. According to Jackson (1969), $\bar{\tau}$ may vary from 10^{-12} seconds for thermoelastic relaxation to 10^{8} seconds for relaxation caused by macroscopic diffusion. Relaxation mechanisms then introduce into the inversion process a great deal of flexibility, but by the same token they reduce the uniqueness of any model that fits a given set of observations.

Two relaxation mechanisms have been used to explain observed surface wave attenuation. Jackson (1969) invoked a thermally activated mechanism where

$$\bar{\tau} = \tau_o \exp(E^* + PV^*)/RT \qquad (15)$$

Here τ_o is a constant, E^* is an activation energy, V^* is an activation volume, P is pressure, T is absolute temperature and R is the gas constant. Solomon (1971) generalized a theory of Walsh (1968, 1969) that relies upon the mechanical effects of a two phase system in a partial melt. Here $\bar{\tau} = \eta/\alpha\mu$, where η is the effective viscosity of the melt, μ the shear modulus of the melt phase, and α is the ratio of minor to major axes of the melt or liquid inclusions.

An important aspect of a relaxation mechanism is that not only is Q^{-1} frequency dependent but so is the effective or real part of the complex modulus in equation (12). Since this is the part of the modulus that determines the velocity of elastic wave propagation, a frequency dependent velocity is called for; maximum when M_U is the effective modulus and minimum when M_R is the effective modulus. Using Walsh's theory and laboratory experiments on rocks whose cracks were filled

with air, water and glycerol, Nur and Simmons (1970) and Nur (1971) invoked partial melting to explain the existence of the low velocity zone. Making use of experiments on an ice-brine system Spetzler and Anderson (1968) and Anderson and Spetzler (1970) presented the same general hypothesis. Relaxation mechanisms may prove to be of great importance in explaining the low velocity zone. In the inversion of surface wave data, however, care must be taken to use the required frequency dependent velocity models of the earth and their partial derivatives in equations (8) or (11), or one must convince oneself that these velocities and their derivatives vary only slightly from those of the usual frequency independent velocity models.

In this study the main emphasis is placed upon the simpler assumption of frequency independent intrinsic attenuation ($10,000/Q_\beta$). Intrinsic attenuation models based upon relaxation mechanisms are also postulated but are not emphasized because: 1) the combination of increased non-uniqueness (brought about by the introduction of relaxation mechanisms), with the quantitative unreliability of the observational data discussed in the previous sections, seriously limits the value of any derived intrinsic attenuation model; 2) the unavailability of frequency dependent velocity models and their partial derivatives (required by the introduction of relaxation mechanisms) results in the highly questionable use of frequency independent velocity models and their partial derivatives in equation (11) when computing the resultant Rayleigh wave attenuation from an intrinsic attenuation model based upon relaxation mechanisms. The abundance of experimental data supporting frequency independent intrinsic attenuation (e.g., Knopoff, 1964; Attewell and Ramana, 1966) makes its emphasis an acceptable alternative.

GENERAL COMMENTS ON FITTING INTRINSIC ATTENUATION MODELS TO THE OBSERVED RAYLEIGH WAVE ATTENUATION

The usual method for determining a model to fit observations involves computing a standard error, or similar statistical measure, beyond which a model generated value should not deviate from the observed value (in this case $10,000/Q_R$). In this study large variations in observed $10,000/Q_R$, often exceeding an order of magnitude, and the relatively few number of observations ruled out meaningful use of such measures. The most consistent aspect of the observations was the confining of the relative peaks of attenuation to different specific period ranges for the different regions across which attenuation was measured. In determining suitable intrinsic attenuation models, the ability of these models to produce peaks of $10,000/Q_R$ in the same period ranges as the observations was the 'best fit' criterion used.

At first an attempt was made to use a least squares method. Data sets used were: 1) averages of $10,000/Q_R$ for a specific region, and 2) simplified models of $10,000/Q_R$ with peaks in the period ranges observed for that particular region (see Figure 11).

If Q is the vector of average or simplified values of $10,000/Q_R$, A is the matrix of the weighting function (that part enclosed in brackets in equation (11)), and q is the vector of $10,000/Q_\beta$ for the different layers, we may write equation (11), multiplied by 10,000, as

$$Q = Aq \tag{16}$$

The solution vector $\tilde{q}$ that will yield values of $10,000/Q_R$ that deviate from the average or simplified values of $10,000/Q_R$ in the least squares sense can be found from

$$\tilde{q} = (A^T A)^{-1} A^T A Q \qquad (17)$$

where $(\ )^T$ indicates a matrix transpose and $(\ )^{-1}$ a matrix inverse. All the solution vectors $\tilde{q}$ computed contained some negative values. Various assumptions as to frequency independence and frequency dependence failed to remove these negative values. While it was possible to obtain a good fit to the average or simplified $10,000/Q_R$ (particularly when a combination of frequency independent and frequency dependent $10,000/Q_\beta$ was allowed), the possibility of negative $10,000/Q_\beta$ was ruled out in this study. A layer having negative intrinsic attenuation requires enhancement rather than dissipation of elastic energy in that layer.

In order to introduce the requirement that all $10,000/Q_\beta$ be positive, a linear programming technique (Hall, McWhorter and Spivey, 1971) was used with a modification suggested by Wagner (1959) that computed models which minimized the sum of absolute deviations from the observed $10,000/Q_R$. These models tended to produce $10,000/Q_R$ that were mean values of the peaks and troughs of the averaged or simplified data sets and failed to satisfy the criteria of reproducing peaks of $10,000/Q_R$ in specified period ranges.

Numerical experiments were then conducted assuming values of $10,000/Q_\beta$ and comparing the resultant $10,000/Q_R$ with the observed $10,000/Q_R$. Varying amounts of success were achieved for the different regions. These results are discussed below. In general, peaks of relative attenuation were reproduced and were made to fall in the proper period ranges; however, the relief, or relative difference between peak and trough was often so small as to question the adequacy of the model.

Backus and Gilbert (1968, 1970) and Jordan and Franklin (1971) have formulated an elegant technique for the inversion of any set of

gross earth data. Again, large variations in the observed values of $10,000/Q_R$ and the inability to compute meaningful statistical measures of these variations as required by the technique precluded its use in this study.

MODELS OF INTRINSIC ATTENUATION FOR SELECTED REGIONS OF NORTH AMERICA

For each region a suitable velocity model was chosen to determine the values of α_n, β_n, c, $\frac{\partial c}{\partial \alpha}_n$, and $\frac{\partial c}{\partial \beta}_n$ to be used in equation (11). In the modeling experiments described below, emphasis was placed on reproducing patterns of relative peaks of attenuation ($10,000/Q_R$) at periods less than 35 seconds.

These regional models of intrinsic attenuation should only be considered as qualitative sketches of relatively high and low intrinsic attenuation ($10,000/Q_\beta$) in the crust and uppermost mantle. The absolute values of $10,000/Q_\beta$ or the thicknesses of the zones of relatively high or low $10,000/Q_\beta$ suggested in these models are not meant to be statistically meaningful quantities. Additional investigations suggested at the end of this paper could lead to more reliable quantitative estimates of intrinsic attenuation for the regions studied.

Eastern Canadian Shield

The CANSD model of Brune and Dorman (1963) was the first velocity model used for the Eastern Canadian Shield. Table 3 and Figure 13 show a frequency independent intrinsic attenuation model and resultant $10,000/Q_R$ that came closest to reproducing the pattern of the simplified data set shown as a dashed line in Figure 13. This model has high intrinsic attenuation at depths of 17 to 35 kilometers and 115 to 215 kilometers. The resulting $10,000/Q_R$ matches the observed pattern of $10,000/Q_R$ with respect to the peak in the 18 to 21 second period range but does not duplicate the 29 to 32 second peak. Similarly a model with high intrinsic attenuation at depths of 6 to 16 kilometers and 35 to 115 kilometers duplicated the high observed attenuation in the 29 to 32 second period range but failed to match the 18 to 21 second peak of observed $10,000/Q_R$. The offset of the peaks and the thickness of the

TABLE 3

Frequency Independent Intrinsic Attenuation Model of the Eastern Canadian Shield (CANSD-1)

Depth (km)	$10,000/Q_\beta$
0 - 6	15
6 - 16.5	8
16.5 - 35.2	120
35.2 - 115.2	60
115.2 - 215.2	200
215.2 - 315.2	20

TABLE 4*

Shear Velocities From CANSD and McEvilly's Central U.S. Canadian Shield Model (MUSCD)

CANSD			MUSCD		
Layer #	Thickness (km.)	Shear Velocity (km/sec)	Layer #	Thickness (km.)	Shear Velocity (km/sec)
1	6	3.47	1	11	3.50
2	10.5	3.64	2	9	3.70
3	18.7	3.85	3	18	4.05
4	80	4.72	4	24	4.65
5	100	4.54	5	40	4.78
6	100	4.51	6	180	4.41
7	80	4.76	7	∞	4.80
8	∞	5.12			

* After McEvilly (1964)

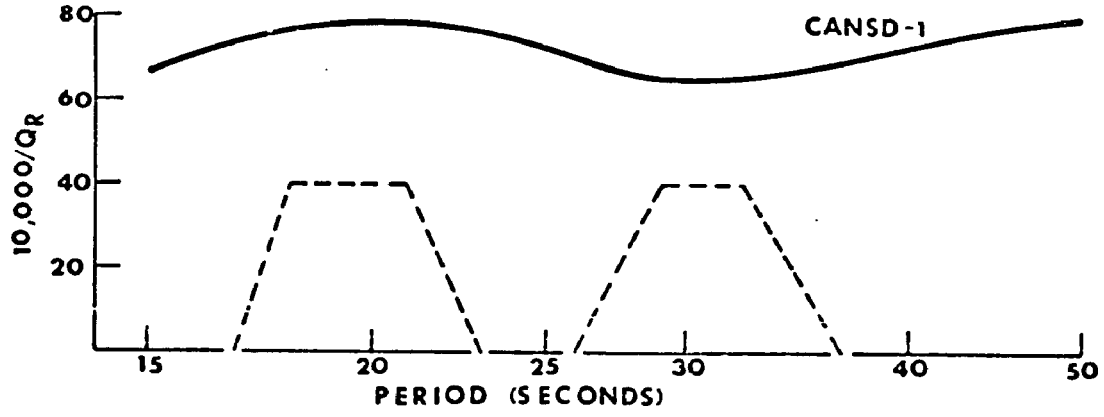


Figure 13. Theoretical $10,000/Q_R$ based on intrinsic attenuation ($10,000/Q_\beta$) model CANSD-1 compared with the Eastern Canadian Shield $10,000/Q_R$ pattern shown as a dashed line.

uppermost mantle layers in the CANSD model (80 and 100 kilometers) suggested that perhaps a finer structure than that implied by this velocity model would allow better fitting of an intrinsic attenuation model.

McEvilly (1964) determined a velocity model for Central United States crust - upper mantle structure whose shear velocities could be perturbed to yield model Rayleigh and Love wave phase velocities that provided a good fit to observed Canadian Shield Rayleigh and Love wave phase velocities. The shear velocity structure he arrived at is very similar to CANSD (see Table 4). Of importance, however, is that layer 4 of CANSD is replaced by two thinner layers (24 and 40 kilometers thick) of approximately the same shear wave velocity. These derived shear wave velocities, compressional wave velocities modified to approximate those of CANSD, CANSD phase velocities and partial derivatives of the original Central United States crust - upper mantle model were used in an attempt to derive a frequency independent intrinsic attenuation model for the Eastern Canadian Shield that would better match the observed $10,000/Q_R$ pattern. Table 5 and Figure 14 show such a model (MUSCD-1) and its derived $10,000/Q_R$, the peaks of which do match the observed pattern. This model has high intrinsic attenuation at depths of 20 to 38 kilometers and 62 to 102 kilometers. The relief or relative difference between peaks and troughs, however, is very small (8%). An attempt to increase this relief by introducing general relaxation mechanisms into the layers of high intrinsic attenuation brought no marked improvement (see MUSCD-2 in Table 6 and Figure 14). A slight increase in relief might result if a finer and/or more accurate velocity structure and resultant partial derivatives were used. However, it is beyond the capability of the $10,000/Q_R$ measurements and their related attenuation patterns to improve upon a suggested velocity structure through a comparison of the quality of fit (e.g., increase in relief of model generated $10,000/Q_R$) obtained using different velocity structures and their related partial derivatives in equation (8) or (11). The large differences in the observed $10,000/Q_R$ for

TABLE 5

Frequency Independent Intrinsic Attenuation Model of the Eastern Canadian Shield (MUSCD-1)

Depth (km)	$10,000/Q_\beta$
0 - 20	20
20 - 38	100
38 - 62	10
62 - 102	120
102 - 282	10

TABLE 6

Intrinsic Attenuation Model of the Eastern Canadian Shield Assuming Localized General Relaxation Mechanisms (MUSCD-2)

Depth (km)	Frequency Independent $10,000/Q_\beta$	Relaxation Mechanism Parameters*
0 - 11	20	------
11 - 20	20	------
20 - 38	----	$\Delta_T = 200$, $2\pi\bar{\tau} = 19$ sec.
38 - 62	10	------
62 - 102	----	$\Delta_T = 260$, $2\pi\bar{\tau} = 30$ sec.
102 - 282	10	------

* $10,000/Q_\beta = \Delta_T\left(\frac{\omega\bar{\tau}}{1+\omega^2\bar{\tau}^2}\right)$, $\quad \Delta_T = 10{,}000\,\Delta_0$

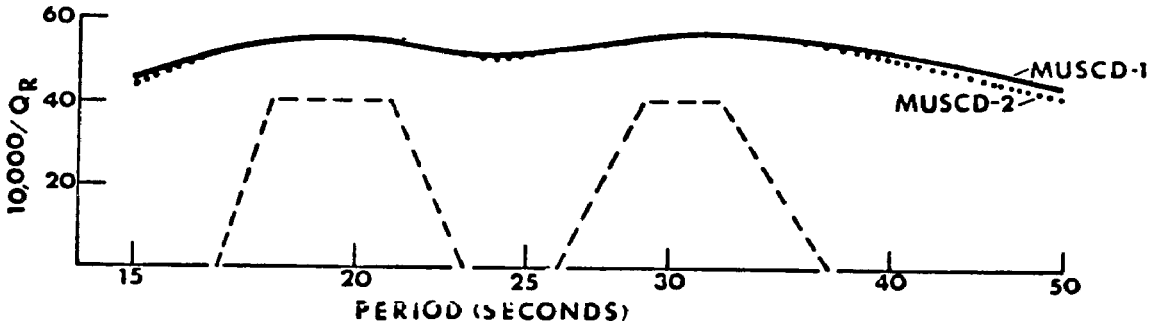


Figure 14. Theoretical $10,000/Q_R$ based on intrinsic attenuation ($10,000/Q_\beta$) models MUSCD-1 and MUSCD-2 compared with the Eastern Canadian Shield $10,000/Q_R$ pattern shown as a dashed line.

different periods must be at least partially due to some other factor, apparently unrelated to the anelastic properties of the earth.

It should be noted that the upper mantle zone of high intrinsic attenuation (layer 5 in MUSCD) corresponds to the higher velocity lid over the low velocity zone. If $10,000/Q_R$ decreases and then increases with period in the 35 to 50 second period range, a zone of lower intrinsic attenuation underlain by a zone of higher intrinsic attenuation may be implied for the mantle below depths of 100 kilometers. If $10,000/Q_R$ remains at a high level or continues rising at periods greater than 32 seconds, high intrinsic attenuation continues on into the low velocity zone.

A thermally activated relaxation mechanism was also assumed and used in a model based on the CANSD velocity structure. The parameters were those of Model 10-04 of Jackson (1969) and the pressure distribution with depth was that of Bullen (1963). Temperature profiles used were a shield model based on Hyndman et al. (1968) and Ringwood (1964), and the convecting model of Stacey (1969). The computed $10,000/Q_R$ for these models are shown in Figure 15 and indicate only a general increase in attenuation with period.

The general relaxation mechanisms described in Table 6 may be converted to thermally activated relaxation mechanisms by means of equation (15). The conversion does not always yield realistic results, e.g., using the relaxation times in Table 6, the parameters of model 10-04 yield a temperature drop of more than $400^{\circ}K$ in going from the shallower to the deeper layers of high intrinsic attenuation. This author is not familiar with any studies which allow for such a temperature inversion. Although all possible models based upon acceptable temperature profiles, pressure profiles, and thermal relaxation parameters (τ_o, E*, V*) have not been tried, it seems unlikely that a thermally activated relaxation mechanism alone, as described by equation (15), could account for the multiple peaks and troughs of the observed attenuation patterns discussed in this study.

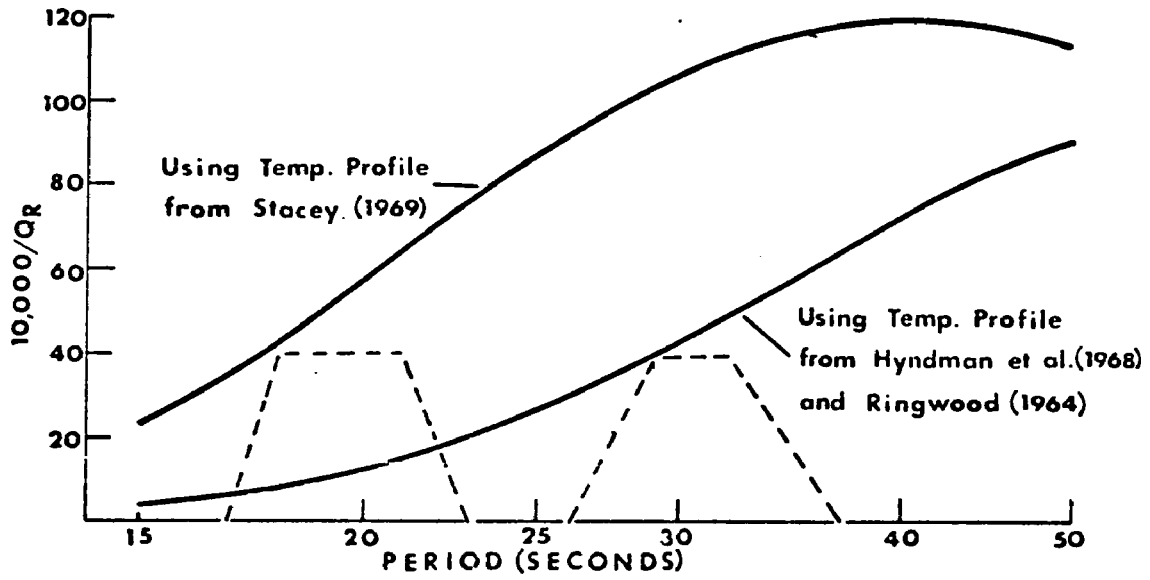


Figure 15. Theoretical 10,000/Q_R based on thermally activated intrinsic attenuation (10,000/Q_β) models compared with the Eastern Canadian Shield 10,000/Q_R pattern shown as a dashed line.

Basin and Range

An examination of some postulated shear velocity structures for the Basin and Range province (Smith, 1962; Alexander, 1963; Kovach and Robinson, 1969) suggested that the Gutenberg Continental model (Takeuchi, Dorman, and Saito, 1964) would represent an average Basin and Range velocity model (see Figure 16 for a comparison). Table 7 and Figure 17 show a frequency independent intrinsic attenuation model (BR-1) and resultant $10,000/Q_R$ that reproduced the pattern of the simplified data set shown as a dashed line in Figure 17. This model has high intrinsic attenuation centered at depths of 10 kilometers and 47 kilometers. As in the Eastern Canadian Shield MUSCD model described above the relief of the resultant $10,000/Q_R$ curve is small. Introducing general relaxation mechanisms into the layers of high intrinsic attenuation increases this relief somewhat (model BR-2 in Table 8 and Figure 17).

It must be reemphasized that the thicknesses of the high attenuation layers (6 kilometers) are not considered to be significant estimates. More accurate determination of the velocity structure and delineation of the actual attenuation mechanism might change these appreciably. As in the previous model the upper mantle zone of high intrinsic attenuation corresponds to the lid of the upper mantle low velocity zone. Again lack of consistency at periods greater than 35 seconds preclude determining whether the low velocity zone itself will also be characterized by high intrinsic attenuation.

Southern Rockies

There are few published velocity models of the Rocky Mountain region. In a recent summary of surface waves and crustal types (Brune, 1969), the Rocky Mountain region would be classified as an Alpine crustal type. In another review (Dorman, 1969), lack of Rayleigh wave data restricted to the Rocky Mountain region alone resulted in a combined Rocky Mountain - Basin and Range classification appearing in plots

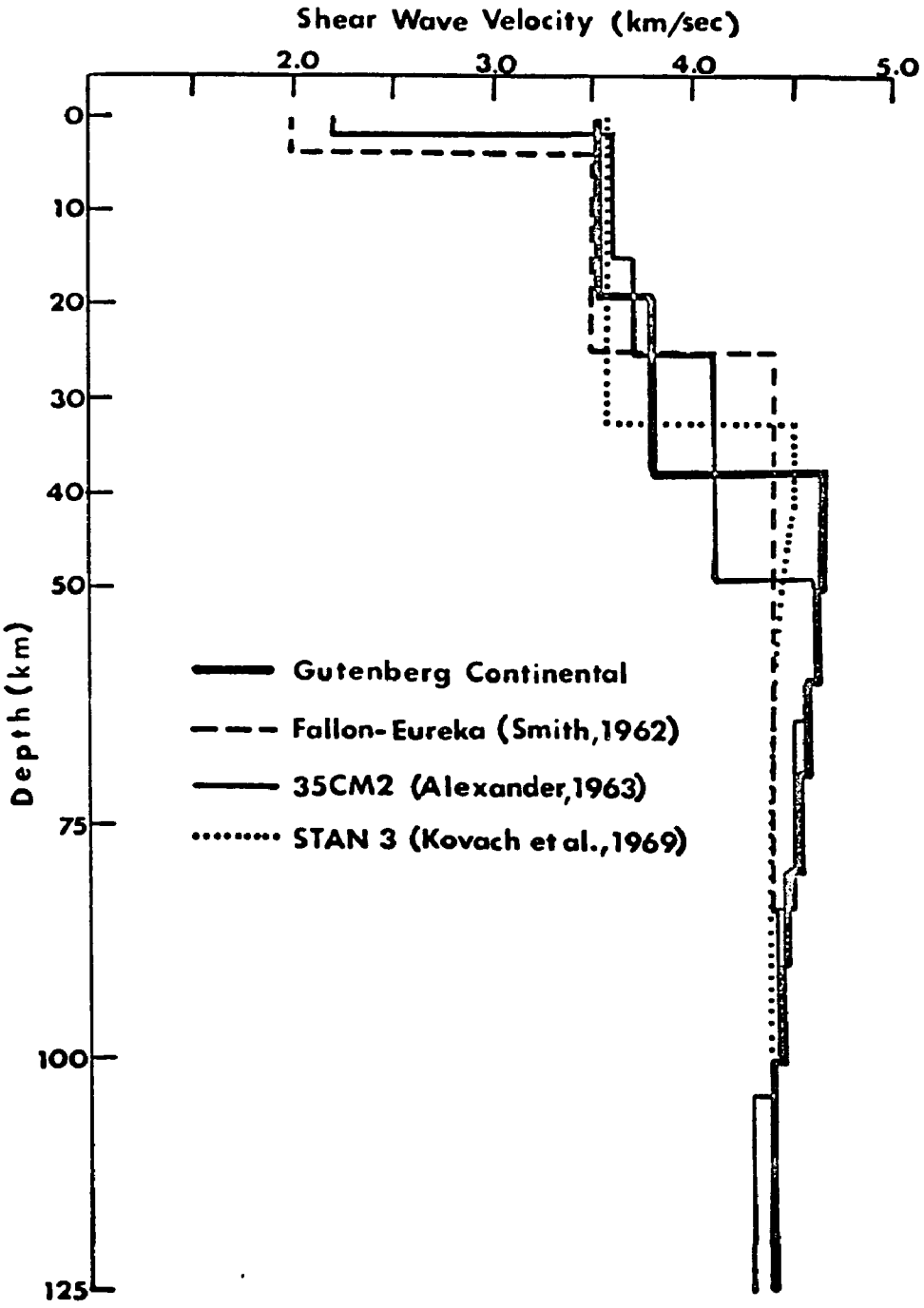


Figure 16. Suggested shear wave velocity models of the Basin and Range compared with the Gutenberg Continental model.

TABLE 7

Frequency Independent Intrinsic Attenuation Model of the Basin and Range (BR-1)

Depth (km)	$10,000/Q_\beta$
0 - 6.3	10
6.3 - 12.6	400
12.6 - 44	10
44 - 50	790
50 - 225	10

TABLE 8

Intrinsic Attenuation Model of the Basin and Range Assuming Localized General Relaxation Mechanisms (BR-2)

Depth (km)	Frequency Independent $10,000/Q_\beta$	Relaxation Mechanism Parameters
0 - 6.3	10	-------
6.3 - 12.6	-------	$\Delta_\tau = 6000$, $2\pi\bar{\tau} = 1$ sec.
12.6 - 44	10	-------
44 - 50	-------	$\Delta_\tau = 1900$, $2\pi\bar{\tau} = 18$ sec.
50 - 225	10	-------

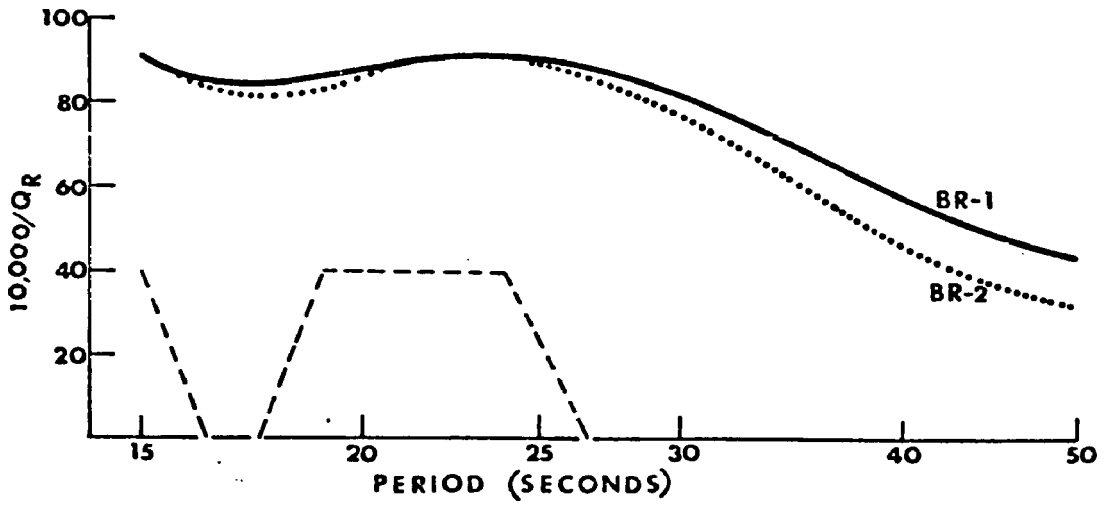


Figure 17. Theoretical $10,000/Q_R$ based on intrinsic attenuation ($10,000/Q_\beta$) models BR-1 and BR-2 compared with the Basin and Range $10,000/Q_R$ pattern shown as a dashed line.

of regional phase velocity data. Consequently, the general Gutenberg Continental model mentioned above was considered to be an adequate velocity model of the Southern Rockies for the purposes of this study. The main difference between this model and shear velocity models of the Alps (e.g., Knopoff, Mueller and Pilant, 1966; Seidl, Müller and Knopoff, 1966) is a deeper onset (80 kilometers vs. 50 kilometers) of the upper mantle low velocity zone in the latter models.

The ambiguity of the pattern of relative peaks of attenuation for this region has previously been mentioned. Models of intrinsic attenuation were constructed in an attempt to match the two simplified $10,000/Q_R$ models shown in Figure 11. It was not possible to duplicate both the 25 to 28 second peak and the 39 to 40 second peak of $10,000/Q_R$ in model RMA. Since peaks greater than 35 seconds were previously found to be inconsistent, effort was concentrated on duplicating the 25 to 28 second peak alone. Table 9 and Figure 18 show a frequency independent intrinsic attenuation model (RMA-1) and resultant $10,000/Q_R$ that match the pattern of model RMA. High intrinsic attenuation is centered at depths of 10 and 55 kilometers. The relief is still small but greater than for the models of the Eastern Canadian Shield or the Basin and Range. The introduction of relaxation mechanisms allows for a slight deepening of these layers (model RMA-2 in Table 10 and Figure 18) or increased relief (model RMA-3 in Table 10 and Figure 18) in the resultant $10,000/Q_R$.

Table 11 and Figure 19 show a frequency independent intrinsic attenuation model (RMB-1) and resultant $10,000/Q_R$ that fit the simplified $10,000/Q_R$ model RMB shown in Figure 11. High intrinsic attenuation is concentrated at depths of 10 and 65 kilometers. Some models allowing for relaxation mechanisms (RMB-2, RMB-3) are listed in Table 12 and their resultant $10,000/Q_R$ are also shown in Figure 19.

In the models of intrinsic attenuation for the Southern Rockies the upper mantle zone of high intrinsic attenuation varies in depth from

50 to 70 kilometers. This is at the same depth as the top of the low velocity zone in the Gutenberg Continental velocity model and the lid over the low velocity zone in the previously mentioned shear velocity models of the Alps.

TABLE 9

Frequency Independent Intrinsic Attenuation Model of the Southern Rockies (RMA-1)

Depth (km)	$10,000/Q_\beta$
0 - 6.3	10
6.3 - 12.6	400
12.6 - 50	10
50 - 60	500
60 - 225	10

TABLE 10

Intrinsic Attenuation Models of the Southern Rockies Assuming Localized General Relaxation Mechanisms (RMA-2, RMA-3)

Depth (km)	$10,000/Q_\beta$	Relaxation Mechanism Parameters
	Model RMA-2	
0 - 12.6	10	------
12.6 - 19	290	------
19 - 60	10	------
60 - 70	------	$\Delta_T = 1600$, $2\pi\bar{\tau} = 13$ sec.
70 - 225	10	------
	Model RMA-3	
0 - 6.3	10	------
6.3 - 12.6	------	$\Delta_T = 6000$, $2\pi\bar{\tau} = 1$ sec.
12.6 - 50	10	------
50 - 60	------	$\Delta_T = 1100$, $2\pi\bar{\tau} = 24$ sec.
60 - 225	10	------

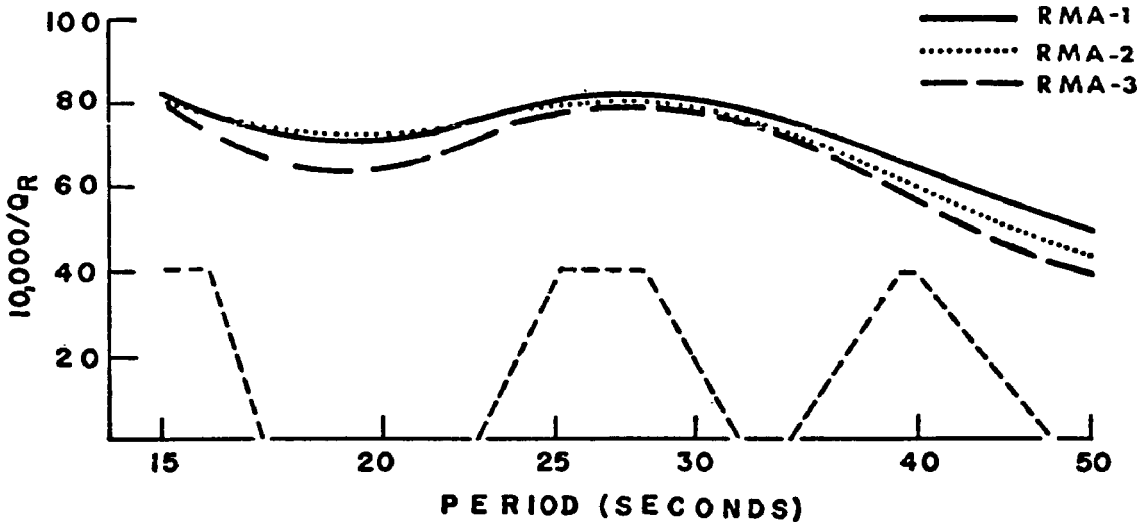


Figure 18. Theoretical $10,000/Q_R$ based on intrinsic attenuation ($10,000/Q_\beta$) models RMA-1, RMA-2, and RMA-3 compared with the Southern Rockies $10,000/Q_R$ pattern (RMA) shown as a dashed line.

TABLE 11

Frequency Independent Intrinsic Attenuation Model of the Southern Rockies (RMB-1)

Depth (km)	$10,000/Q_\beta$
0 - 6.3	10
6.3 - 12.6	400
12.6 - 60	10
60 - 70	600
70 - 225	10

TABLE 12

Intrinsic Attenuation Models of the Southern Rockies Assuming Localized General Relaxation Mechanisms (RMB-2, RMB-3)

Depth (km)	$10,000/Q_\beta$	Relaxation Mechanism Parameters
	Model RMB-2	
0 - 12.6	10	------
12.6 - 19.0	290	------
19 - 60	10	------
60 - 70	------	$\Delta_T = 1250$, $2\pi\bar{\tau} = 45$ sec.
70 - 225	10	------
	Model RMB-3	
0 - 6.3	10	------
6.3 - 12.6	------	$\Delta_T = 6000$, $2\pi\bar{\tau} = 1$ sec.
12.6 - 50	10	------
50 - 60	------	$\Delta_T = 1850$, $2\pi\bar{\tau} = 90$ sec.
60 - 225	10	------

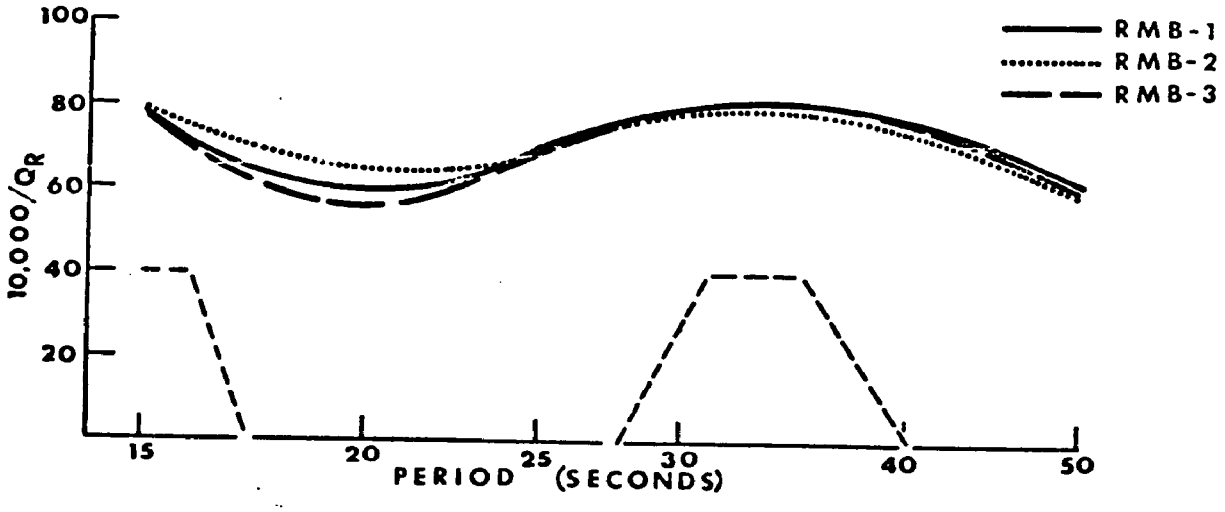


Figure 19. Theoretical $10,000/Q_R$ based on intrinsic attenuation ($10,000/Q_\beta$) models RMB-1, RMB-2, and RMB-3 compared with the Southern Rockies $10,000/Q_R$ pattern (RMB) shown as a dashed line.

INTERPRETATION OF INTRINSIC ATTENUATION MODELS

In all of the intrinsic attenuation models discussed above, both crustal and upper mantle zones of high attenuation are present. These zones are necessary when frequency independent intrinsic attenuation is assumed in fitting regional models to the simplified data sets. The assumption of intrinsic attenuation due to relaxation mechanisms, however, has as yet an undetermined effect upon the uniqueness of any particular model. Information aside from that determined from Rayleigh wave observations is necessary to limit the choice of models if this last assumption is to be made.

Figure 20 summarizes schematically the models of frequency independent intrinsic attenuation for the regions studied. A comparison of these models suggests deepening of the zones of high intrinsic attenuation in the transition from the Basin and Range to the Canadian Shield. The corresponding regional decrease in surface heat flow mentioned previously again suggests that these zones may be related to thermal properties. Specific aspects of the crustal zone and upper mantle zone of high intrinsic attenuation are discussed below.

Crustal Zone of High Intrinsic Attenuation

Models of the intrinsic attenuation properties of the earth based on long period surface wave or free oscillation measurements contain little information about the distribution of these properties within the crust. Model MM8 of Anderson, Ben-Menahem and Archambeau (1965) utilizes a crust with relatively low intrinsic attenuation ($Q_\beta = 450$, $10,000/Q_\beta = 22$). This value was taken from the determination of Q for Lg waves (Press, 1964). Using data taken from Q measurements of Love and Rayleigh waves in the 15 to 50 second period range, Tsai and Aki (1969) proposed a model with intrinsic attenuation increasing towards the earth's surface from a depth of 50 kilometers. Tsai and Aki (1969) also computed a simple two component frequency dependent intrinsic

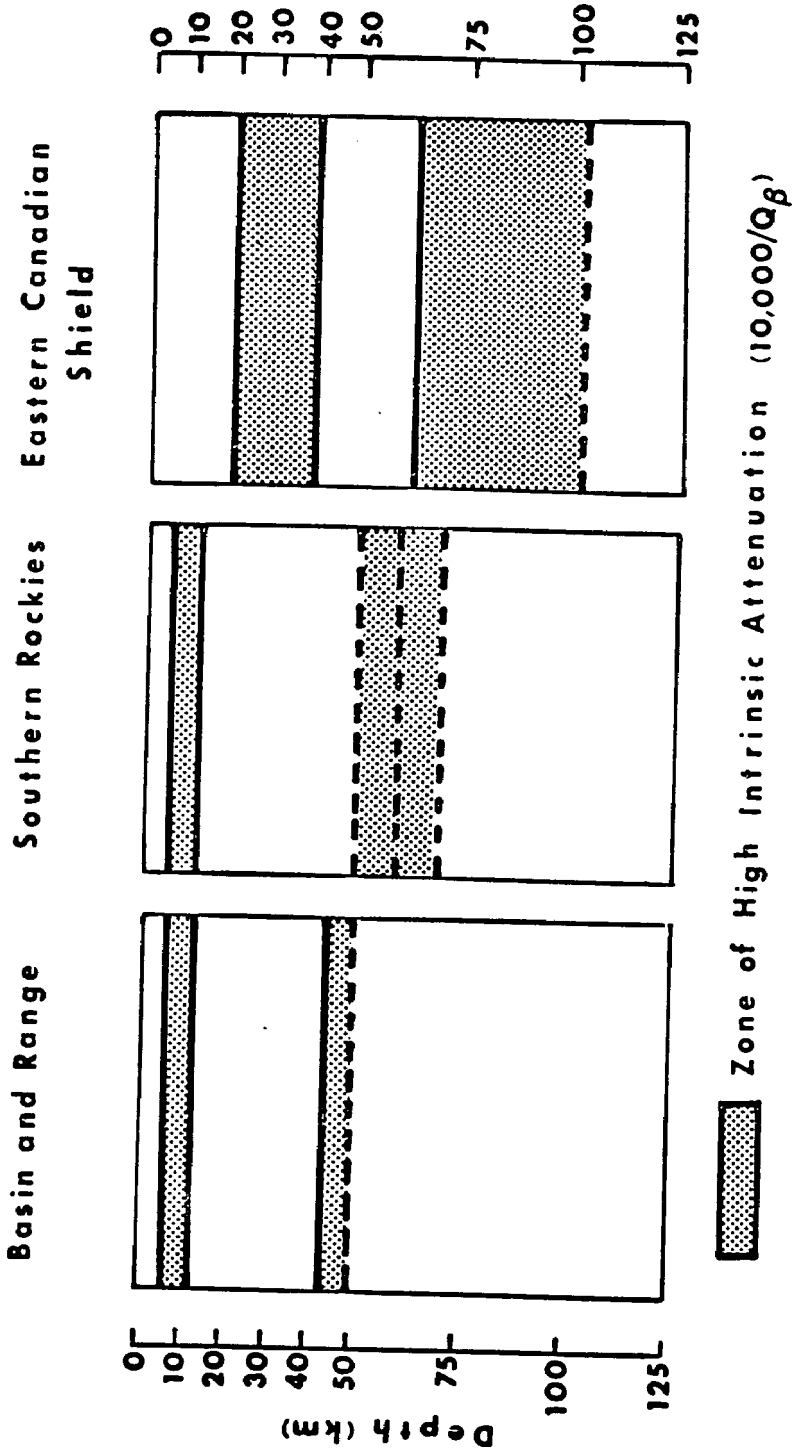


Figure 20. Schematic frequency independent intrinsic attenuation ($10,000/Q_\beta$) models of the Eastern Canadian Shield, the Southern Rockies and the Basin and Range.

attenuation model which allowed them to better match the 'relief' of observed surface wave attenuation. This model also stipulates high intrinsic attenuation (for the higher frequencies) in the upper crust. Solomon (1971), relying mostly on attenuation measurements of Love and Rayleigh waves at periods less than 100 seconds, postulated a low attenuating lithosphere for both Western and East Central United States. He also suggested that in both regions the upper part of the lithosphere might possibly have higher intrinsic attenuation than the lower part.

Models of the intrinsic attenuation properties of the crust based on body wave measurements are not abundant in the literature. The acknowledged presence of widespread lateral inhomogeneities in the crust and the relatively short wave length of body waves suggest that scattering may be an important factor in any attenuation measurement. Recently, regional models were suggested by Clowes and Kanasewich (1969) and Fedotov and Boldyrev (1969). Clowes and Kanasewich (1969), restricting themselves to compressional waves, postulated low intrinsic attenuation ($Q_\alpha = 1500$, $10,000/Q_\alpha = 6.7$) for the bottom 40 kilometers of the crust in southern Alberta. They also suggested greater variations and relatively higher average intrinsic attenuation ($Q_\alpha = 300$, $10,000/Q_\alpha = 33.3$) for the upper two kilometers of the crust in the same region. Fedotov and Boldyrev (1969), examining earthquakes in the Kurile Island region, found a frequency dependence in the attenuation properties of both compressional and shear waves. In their model, intrinsic attenuation is relatively high ($Q_\beta = 86$, $10,000/Q_\beta = 116$) for 1.25 Hz shear waves at depths between 25 and 55 kilometers. At 20 Hz this zone of relatively high intrinsic attenuation has shifted upward to depths between 5 and 25 kilometers. At this higher frequency, however, attenuation in this zone is generally lower (i.e., $Q_\beta = 270$ and $10,000/Q_\beta = 37$).

In this study high intrinsic attenuation in the crust occurs at depths of 6 to 13 kilometers for the Basin and Range and Southern Rockies models and 20 to 38 kilometers for the Eastern Canadian Shield model. None of the velocity models used in the calculations discussed in

the previous section contain crustal low velocity zones. These zones, however, have been suggested by some seismologists for different parts of the crust. Gutenberg (1951, 1954) was the first to postulate the existence of a crustal low velocity zone. He summarized his observations by stating (Gutenberg, 1959), '... combined evidence from travel times, laboratory experiments and data on channel waves in the crust favors the hypothesis that below a locally variable depth, probably roughly 10 kilometers, but different for longitudinal and transverse waves and for different materials, the wave velocities begin to decrease with increasing depth...' More recently Mueller and Landisman (1966) and Landisman and Mueller (1966), citing observations from continental regions around the world, suggested a low velocity zone for compressional waves existing at depths between 6 and 10 kilometers.

Landisman, Mueller and Fuchs (1967) and Closs (1969) cited further examples of postulated crustal low velocity zones in Western Europe at depths ranging from 8 to 20 kilometers. Sellevol et al. (1971) postulated a low velocity zone for compressional waves, 5 to 15 kilometers deep, beneath the Paleozoic Caledonides of Western Norway. Lukk, Nersesov, and Chepkunas (1970) found evidence for a low velocity zone for both compressional and shear waves at depths between 15 and 25 kilometers beneath the mountainous Garm district in Central Asia. Pavlenkova (1969) suggested a low velocity zone for compressional waves at depths between 25 and 30 kilometers beneath the Ukrainian Shield.

In North America, Press and Biehler (1964) postulated a low velocity zone beneath the Sierra Nevada beginning at a depth of 5 kilometers. Prodehl (1970) suggested thin low velocity zones for compressional waves at depths of 20 and 25 kilometers beneath the middle Rocky Mountains and the Southern Cascades. Mitchell and Landisman (1970) postulated a low velocity zone for compressional waves at depths between 15 and 18 kilometers beneath Oklahoma. Kanasewich and

Cumming (1965) postulated a low velocity zone for compressional waves at depths between 23 and 34 kilometers beneath southern Alberta. Similarly, Wickens and Pec (1968), in analyzing Love waves suggested a low velocity zone for shear waves at depths between 20 and 35 kilometers beneath the Northern Canadian Shield.

Other investigators (e.g., Kosminskaya, Belyaevsky and Volvovsky, 1969; Brune, 1969), while not finding direct evidence for the existence of low velocity layers in the crust indicate that their existence is quite a reasonable assumption. Consequently, if the assumption is made that there do exist low velocity layers in the crust beneath North America at depths similar to those described above, then the crustal zones of high intrinsic attenuation shown in Figure 20 would occur at the same depths or immediately above these layers.

Additional evidence for the existence of crustal low velocity zones beneath North America would enable us to determine the similarity to and differences between the crustal zone of high intrinsic attenuation discussed in this section and the upper mantle zone of high intrinsic attenuation discussed in the following section. The interrelation of high intrinsic attenuation and low seismic velocity is an essential part of several suggested attenuation mechanisms, particularly partial melting (Walsh, 1969; Nur, 1971).

Upper Mantle Zone of High Intrinsic Attenuation

An integral part of all suggested models of intrinsic attenuation in the earth is an upper mantle zone of high intrinsic attenuation. Model MM8 (Anderson, Ben-Menahem and Archambeau, 1965) shows a peak of intrinsic attenuation ($10,000/Q_\beta = 167$) at depths between 38 and 60 kilometers. Tsai and Aki's model (Tsai and Aki, 1969) has its highest intrinsic attenuation ($10,000/Q_\beta = 182$) at depths between 100 and 200 kilometers. Since Tsai and Aki's model was determined from the attenuation of surface waves in the 15 to 50 second period range and model MM8 from the attenuation of free oscillations and surface waves

greater than 50 seconds, frequency dependent intrinsic attenuation may be indicated. At these depths relative pressure is small and increasing temperature would decrease the relaxation times of a thermally activated relaxation mechanism (see equation (15) and Gordon and Nelson, 1966). Consequently, as the period of the seismic wave used in the inversion decreases, intrinsic attenuation would be found to peak at greater temperatures and hence greater depths.

Solomon (1971) has proposed a relaxation mechanism for upper mantle attenuation beneath the Western United States. He suggests dual relaxation times ($2\pi\bar{\tau}$) of 0.05 seconds and 125.0 seconds for depths between 64 and 160 kilometers to simultaneously account for short period (1 second) body wave low velocity zones and surface wave attenuation. At depths between 160 and 350 kilometers he postulates a relaxation time of 12.5 seconds to account for the attenuation of 10 second shear waves. For the East Central United States, he suggests that the upper mantle zone of high intrinsic attenuation is less pronounced and deeper, beginning at depths of 100 to 120 kilometers.

Intrinsic attenuation models based on compressional body wave measurements alone have also included zones of high intrinsic attenuation at different depths in the upper mantle. Teng (1968) suggested a model based on long period (5 to 100 seconds) body waves which exhibits a peak of intrinsic attenuation ($10,000/Q_\alpha = 167$) at depths between 36 and 50 kilometers. Kanamori (1967), using short period (approximately 1 second) body waves, derived a similar model, while Archambeau, Flinn and Lambert's model (Archambeau et al., 1969), also derived from short period body waves, exhibits a peak of intrinsic attenuation ($10,000/Q_\alpha = 71$) at depths between 82 and 100 kilometers.

The integration of the above models and those suggested in this study into an all-inclusive, regionally variable, frequency dependent phenomenological model of intrinsic attenuation in the upper mantle would be of great importance. However, the relatively unknown observational errors at different frequencies, and the unknown effects of

attenuation not due to anelastic properties would greatly minimize the reliability of any such computed model.

Figure 20 shows the depths of maximum intrinsic attenuation in the upper mantle suggested in this study. The zone of high or highest intrinsic attenuation in the upper mantle occurs at a depth of 44 to 50 kilometers for the Basin and Range model and either 50 to 60 or 60 to 70 kilometers for the Rocky Mountains model. The Eastern Canadian Shield model has high intrinsic attenuation at depths between 62 and 102 kilometers. These variations in depth (44 to 102 kilometers) all lie within the range of depths for upper mantle zones of maximum intrinsic attenuation (36 to 200 kilometers) described in previous models mentioned above. Specific differences between the intrinsic attenuation models presented in this study and those of other investigators may be due to several reasons: 1) other investigators usually based their models upon averaged data sets representing attenuation measurements from diverse regions; 2) among these measurements, surface wave attenuation was sometimes determined when the azimuthal difference between great circle propagation paths was several degrees (i.e., $\Delta AZ > 1^{o}$); 3) other investigators emphasized the absolute values of their attenuation measurements, e.g., the 'fit' of an intrinsic attenuation model was determined by how well the values of surface wave attenuation predicted by the model fit within statistically determined error limits of the averaged observations. In this study it is felt that a regionally repeated qualitative pattern of relatively high and low attenuation, determined from surface wave measurements at station pairs where $\Delta AZ < 1^{o}$, is the most reliable aspect of the observations.

While the lack of consistent patterns of attenuation at periods greater than 35 seconds disallow any statement about the lower extent of the upper mantle zones of high intrinsic attenuation, it can be said that with the possible exception of the Southern Rockies model, high intrinsic attenuation occurs at the same depth as the higher velocity lid overlying the upper mantle low velocity zone suggested for each region. A detailed

explanation of this phenomena is not offered here; however, some speculation can be attempted. One possible explanation would be a leakage of energy from the lid to the low velocity zone itself. Archambeau, Flinn and Lambert (1969) mentioned this as a possible explanation of observed frequency dependent attenuation in the upper mantle lid beneath Western United States. They subsequently ruled it out in favor of frequency dependent intrinsic attenuation at that depth.

Another explanation is related to relaxation mechanisms. If, because of some factor (e.g., temperature), the relaxation time $\bar{\tau}$ decreases with depth, then for any given frequency ω_o, maximum attenuation is attained at a depth where $\bar{\tau} = 1/\omega_o$, while minimum propagation velocity (i.e., when M_R is the effective modulus) occurs at relaxation time $\bar{\tau} << 1/\omega_o$ or greater depths.

The assumption of some frequency dependent attenuation mechanisms (e.g., relaxation mechanisms) leads to an additional complicating factor, i.e., frequency dependent seismic wave velocities. Velocity models of this type could conceivably result in a decrease or increase in the differences in depth between the low velocity zones and the zones of high intrinsic attenuation.

The mutual occurrence of low velocity zones and zones of high intrinsic attenuation is of importance in the theory of the new global tectonics. Isacks, Oliver and Sykes (1968) believe that the asthenosphere corresponds generally to the upper mantle zone that propagates seismic waves (especially shear waves) at lower velocities and with greater attenuation than the lithosphere (above) or mesosphere (below). Molnar and Oliver (1969) while not being able to define any physical mechanism that equates Q and 'strength' (see also Gordon, 1967) are reassured of this relationship by their belief that the low Q, high attenuating zone is associated with the low velocity zone. They refer to Anderson's (Anderson, 1962) suggestion that the low velocity zone is also a zone of weakness.

A better understanding of the relationship between the attenuation and velocity of seismic waves will play an important role in validating present models of plate tectonics and suggesting new ones.

SUGGESTIONS FOR FUTURE INVESTIGATIONS

1. Additional measurements of Rayleigh wave attenuation across North America are needed to verify the regional patterns of $10,000/Q_R$ outlined in this study. Hopefully, these measurements would also provide sufficient data to employ statistical techniques allowing quantitative estimates of intrinsic attenuation to be made. The added measurement of Love wave attenuation across the same regions would also allow for the separate determination of $10,000/Q_\alpha$ and $10,000/Q_\beta$ or K^* and μ^*. The assumptions made in this study that $K^* = 0$ and that the earth behaves as a Poisson solid are certainly open to question.

2. The determination of attenuation of both Love and Rayleigh waves using high-gain wide-band long-period seismographs such as those described by Pomeroy et al. (1969), with enhanced response in the 30 to 60 second period range, is necessary if we are to have reliable attenuation data at periods greater than 35 seconds. An accurate description of the depth of the upper mantle zone of high intrinsic attenuation can only be determined from measurements in this period range.

3. Increased observational and theoretical investigations into the propagation of surface waves across continental margins, downgoing slabs and other non-layered regions and/or models would enable us to better understand observed surface wave amplitude fluctuations. For studies such as this one, the neutralization of purely geometrical effects upon attenuation is vital if the anelastic properties of the earth are to be determined.

4. The large differences between separate determinations of Rayleigh wave attenuation measured along paths differing only slightly from each other may be attributed at least in part to the sensitivity of seismic wave amplitudes to relatively small differences in local structure or local changes in physical properties. This sensitivity of amplitude to

spatially small structural or property changes has also been observed with regard to small structural or property changes with time. Gowd (1970) stressed rock specimens until they fractured, measuring changes in the velocity and amplitudes of ultrasonic pulses transmitted through the samples at different stress levels. He found that in almost all the samples tested there was a steady increase in the amplitudes of the pulses with increasing stress, until approximately one-half the fracture stress was reached. Amplitudes then started decreasing, first slowly and then sharply until fracture was achieved. Velocity, on the other hand, increased monotonically until fracture was achieved. He suggested that the study of amplitude, or attenuation changes with time may be useful in earthquake prediction.

This author, agreeing with this suggestion, believes that a carefully controlled experiment involving a non-destructive source such as is used in oil exploration, set in line with fixed seismometers on both sides of an active fault, could be an effective monitor of any structural, deformational or stress changes in the fault zone prior to a fault movement or earthquake. The sensitivity of seismic wave amplitudes that was so problematic to the consistent determination of Rayleigh wave attenuation in this study may prove to be beneficial in other areas of seismology.

SUMMARY

1. Attenuation ($10,000/Q_R$) was determined for Rayleigh waves in the 15 to 50 second period range across different structural provinces of North America. Although large variations in the absolute value of $10,000/Q_R$ for a given period were observed, patterns of relative peaks of attenuation were consistent within several regions. Relative peaks of attenuation were observed at periods of 15 seconds and between 19 and 24 seconds for the Basin and Range, at 15 to 16 seconds and between 25 and 28 seconds or 31 and 35 seconds for the Southern Rockies and between 18 and 21 and between 29 and 32 seconds for the Eastern Canadian Shield. At periods greater than 35 seconds patterns were not obvious, although attenuation increasing with period was sometimes indicated. Relative peaks of attenuation shifted to longer periods in the transition from the younger region of higher heat flow (Basin and Range) to the older region of lower heat flow (Canadian Shield).

2. Measurements of Rayleigh wave attenuation along paths crossing the Northwestern Canadian Shield failed to yield consistent patterns of attenuation. This is believed to be due to the lateral refraction of Rayleigh waves caused by postulated deep structural contrasts within this section of the Canadian Shield.

3. Qualitative success was achieved in reproducing patterns of $10,000/Q_R$ by means of regional models of frequency independent intrinsic attenuation ($10,000/Q_\beta$). The relief or relative difference between peaks and troughs of the model determined $10,000/Q_R$ was often so low as to question the adequacy of the models. Assuming intrinsic attenuation due to relaxation mechanisms increased this relief somewhat but also increased the non-uniqueness of any suggested intrinsic attenuation model and required frequency dependence in the assumed velocity models.

4. Frequency independent intrinsic attenuation models exhibited high intrinsic attenuation at depths of 6 to 13 kilometers and 44 to 50 kilometers for the Basin and Range, 6 to 13 kilometers and either 50 to 60 or 60 to 70 kilometers for the Southern Rockies, and 20 to 38 kilometers and 62 to 102 kilometers for the Eastern Canadian Shield. In the different models the crustal zone of high intrinsic attenuation occurred at the same depths as most of the crustal low velocity zones that have been postulated by some seismologists. With the possible exception of the Southern Rockies, the upper mantle zone of high intrinsic attenuation occurred at the same depth as the higher velocity lid overlying the regional low velocity zone accepted by most seismologists. Lack of consistent data at periods greater than 35 seconds precluded determining whether the upper mantle zone of high intrinsic attenuation extends into the upper mantle low velocity zone.

5. Additional data, high-gain long-period seismographs and additional theoretical and observational studies of wave propagation are necessary if regional models of intrinsic attenuation are to be determined more accurately. Attenuation studies are important in validating theories of global tectonics, and may prove relevant to earthquake prediction.

REFERENCES

Alexander, S. S., Surface wave propagation in the western United States, Ph.D. thesis, California Institute of Technology, Pasadena, 242 pp., 1963.

Anderson, D. L., The plastic layer of the earth's mantle, Sci. Am., July 1962.

Anderson, D. L., The anelasticity of the mantle, Geophys. J., 14, 135, 1967.

Anderson, D. L., Latest information from seismic observations, in The Earth's Mantle, ed. by T. F. Gaskell, Academic Press, New York, 355, 1968.

Anderson, D. L., and C. B. Archambeau, The anelasticity of the earth, J. Geophys. Res., 69, 2071, 1964.

Anderson, D. L., A. Ben-Menahem, and C. B. Archambeau, Attenuation of seismic energy in the upper mantle, J. Geophys. Res., 70, 1441, 1965.

Anderson, D. L., and H. Spetzler, Partial melting and the low-velocity zone, Phys. Earth Planet. Interiors, 4, 62, 1970.

Archambeau, C. B., E. A. Flinn, and D. G. Lambert, Fine structure of the upper mantle, J. Geophys. Res., 74, 5825, 1969.

Attewell, P. B., and Y. V. Ramana, Wave attenuation and internal friction as functions of frequency in rocks, Geophysics, 31, 1049, 1966.

Backus, G., and F. Gilbert, The resolving power of gross earth data, Geophys. J. Roy. Astron. Soc., 16, 169, 1968.

Backus, G., and F. Gilbert, Uniqueness in the inversion of inaccurate gross earth data, Phil. Trans. Roy. Soc. London, Ser. A., 266, 123, 1970.

Ben-Menahem, A., Observed attenuation and Q values of seismic waves in the upper mantle, J. Geophys. Res., 70, 4641, 1965.

Bergland, G. D., A guided tour of the fast Fourier transform, IEEE Spectrum, 6, 41, 1969.

Blackwell, D. D., Heat-flow determinations in the northwestern United States, J. Geophys. Res., 74, 992, 1969.

Brigham, E. O., and R. E. Morrow, The fast Fourier transform, IEEE Spectrum, 4, 63, 1967.

Brune, J., Attenuation of dispersed wave trains, Bull. Seism. Soc. Am., 52, 109, 1962.

Brune, J., Surface waves and crustal structure, in The Earth's Crust and Upper Mantle, ed. by P. J. Hart, Amer. Geophys. Un. Geophys. Mon. 13, Washington, D. C., 230, 1969.

Brune, J., and J. Dorman, Seismic waves and earth structure in the Canadian Shield, Bull. Seism. Soc. Amer. 53, 167, 1963.

Bullen, K., An Introduction to the Theory of Seismology, 3rd edition, 381 pp., Cambridge University Press, Cambridge, 1963.

Capon, J., Analysis of Rayleigh wave multipath propagation of LASA, Bull. Seism. Soc. Am., 60, 1701, 1970.

Closs, H., Explosion seismic studies in Western Europe, in The Earth's Crust and Upper Mantle, ed. by P. J. Hart, Amer. Geophys. Un. Geophys. Mon. 13, Washington, D. C., 178, 1969.

Clowes, R. M. and E. R. Kanasewich, Seismic attenuation and the nature of reflecting horizons within the crust, J. Geophys. Res., 75, 6693, 1970.

Cooley, J. W., and J. W. Tukey, An algorithm for the machine calculation of complex Fourier series, Math. Comput., 19, 297, 1965.

Cooley, J. W., P. A. W. Lewis, and P. D. Welch, Application of the fast Fourier transform to the computation of Fourier integrals, Fourier series and convolution integrals, IEEE Trans. Audio and Electroacoustics, AU-15, 79, 1967.

Dorman, J. Seismic surface-wave data on the upper mantle, in The

Earth's Crust and Upper Mantle, ed. by P. J. Hart, Amer. Geophys. Un. Geophys. Mon. 13, Washington, D. C., 257, 1969.

Espinosa, A. F., G. H. Sutton and H. J. Miller, A transient technique for seismograph calibration - manual and standard set of theoretical transient responses, 109 pp., VESIAC Special Report 4410-106-x, Geophys. Lab., Inst. Science and Technol., Univ. of Mich., Ann Arbor, 1965.

Ewing, W. M., W. S. Jardetsky, and F. Press, Elastic Waves in Layered Media, 380 pp., McGraw-Hill, New York, 1957.

Fedotov, S. A., and S. A. Boldyrev, Frequency dependence of the body-wave absorption in the crust and upper mantle of the Kuril-Island chain, Bull. Acad. Sci. USSR, Geophys. Ser., English Transl., no. 9, 553, 1969.

Geotechnical Corp., Calibration of the World-Wide Seismograph System, Appendix A and B, in Operation and Maintenance Manual, World-Wide Seismograph System, Model 10700, Garland, Texas, 1961.

Gordon, R. B., Thermally activated processes in the earth: Creep and seismic attenuation, Geophys. J., 14, 33, 1967.

Gordon, R. B., and C. W. Nelson, Anelastic properties of the earth, Rev. Geophys., 4, 457, 1966.

Gowd, T. N., Changes in absorption of ultrasonic energy travelling through rock specimens stressed to fracture, Phys. Earth Planet. Interiors, 4, 43, 1970.

Gutenberg, B., Revised travel times in Southern California, Bull. Seism. Soc. Am., 41, 143, 1951.

Gutenberg, B., Low-velocity layers in the earth's mantle, Bull. Geol. Soc. Am., 65, 337, 1954.

Gutenberg, B., Physics of the Earth's Interior, 240 pp., Academic Press, New York, 1959.

Hall, W. K., A. McWhorter, and W. A. Spivey, Optimization Programs at the University of Michigan, 47 pp., Graduate School of Business Administration, Univ. of Mich., Ann Arbor, 1971.

Hunter, J. A., and R. F. Mereu, The crust of the earth under Hudson Bay, Can. J. Earth Sci. 4, 949, 1967.

Hyndman, R. D., I. B. Lambert, K. S. Heier, J. C. Jaeger, and A. E. Ringwood, Heat flow and surface radioactivity measurements in the Precambrian shield of Western Australia, Phys. Earth Planet. Interiors, 1, 129, 1968.

Isacks, B., J. Oliver, and L. R. Sykes, Seismology and the new global tectonics, J. Geophys. Res., 73, 5855, 1968.

Jackson, D. D., Elastic relaxation model for seismic wave attenuation in the earth, Phys. Earth Planet. Interiors, 2, 30, 1969a.

Jackson, D. D., and D. L. Anderson, Physical mechanisms of seismic-wave attenuation, Rev. Geophys., 8, 1, 1970.

Jordan, T. H., and J. N. Franklin, Optimal solutions to a linear inverse problem in geophysics, Proc. Nat. Acad. Sci., 68, 291, 1971.

Kanamori, H., Spectrum of P and PcP in relation to the mantle-core boundary and attenuation in the mantle, J. Geophys. Res., 72, 559, 1967.

Kanamori, H., Velocity and Q of mantle waves, Phys. Earth Planet Interiors, 2, 259, 1970.

Kanasewich, E. R. and G. L. Cumming, Near-vertical-incidence seismic reflections from the "Conrad" Discontinuity, J. Geophys. Res., 70, 3441, 1965.

King, P. B., Tectonic map of North America, U.S. Geological Survey, Washington, D.C., G67154, 1969.

Knopoff, L., Q, Rev. Geophys., 2, 625, 1964.

Knopoff, L., K. Aki, C. B. Archambeau, A. Ben-Menahem, and J. A. Hudson, Attenuation of dispersed waves, J. Geophys. Res., 69, 1655, 1964.

Knopoff, L., S. Mueller, and W. L. Pilant, Structure of the crust and upper mantle in the Alps from the phase velocity of Rayleigh waves, Bull. Seism. Soc. Am., 56, 1009, 1966.

Kosminskaya, I. P., N. A. Belyaevsky, and I. S. Volvovsky, Explosion seismology in the USSR, in The Earth's Crust and Upper Mantle, ed. by P. J. Hart, Amer. Geophys. Un. Geophys. Mon. 13, Washington, D. C., 195, 1969.

Kovach, R. L., and R. Robinson, Upper mantle structure in the Basin and Range province, western North America, from the apparent velocities of S waves, Bull. Seism. Soc. Am., 59, 1653, 1969.

Landisman, M., and S. Mueller, Seismic studies of the earth's crust in continents, 2, Analysis of wave propagation in continents and adjacent shelf areas, Geophys. J., 10, 539, 1966.

Landisman, M., S. Mueller, and K. Fuchs, Further evidence for the sialic low-velocity zone in continental areas (abstract), Geophys. J., 13, 367, 1967.

Lukk, A. A., I. L. Nersesov, and L. S. Chepkunas, Procedure for the identification of the low velocity layer in the earth's crust and mantle, Bull. Acad. Sci. USSR, Geophys. ser., English Transl., no. 2, 77, 1970.

McEvilly, T. V., Central U.S. crust-upper mantle structure from Love and Rayleigh wave phase velocity inversion, Bull. Seism. Soc. Am., 54, 1997, 1964.

McGarr, A., Amplitude variations of Rayleigh waves - horizontal refraction, Bull. Seism. Soc. Am., 59, 1307, 1969.

McGinley, J. R., Jr., and D. L. Anderson, Relative amplitudes of P and S waves as a mantle reconnaissance tool, Bull. Seism. Soc. Am., 59, 1189, 1969.

Mereu, R. F., and J. A. Hunter, Crustal and upper mantle structure under the Canadian Shield from Project Early Rise data, Bull. Seism. Soc. Am., 59, 147, 1969.

Mitchell, B. J., and M. Landisman, Interpretation of a crustal section across Oklahoma, Bull. Geol. Soc. Am., 81, 2647, 1970.

Molnar, P., and J. Oliver, Lateral variations of attenuation in the upper mantle and discontinuities in the lithosphere, J. Geophys. Res., 74, 2648, 1969.

Mueller, S., and M. Landisman, Seismic studies of the earth's crust in continents, 1, Evidence for a low-velocity zone in the upper part of the lithosphere, Geophys. J., 10, 525, 1966.

Nur, A., Viscous phase in rocks and the low-velocity zone, J. Geophys. Res., 76, 1270, 1971.

Nur, A., and G. Simmons, The effect of viscosity of a fluid phase on velocity in low porosity rocks, Earth Planet. Sci. Letters, 7, 99, 1969.

Oliver, J., A summary of observed seismic surface wave dispersion, Bull. Seism. Soc. Am., 52, 81, 1962.

Pavlenkova, N. I., Velocity profile of the earth's crust in the central Ukraine, Bull. Acad. Sci. USSR, Geophys. Ser. English Transl., no. 6, 346, 1969.

Pilant, W. L., and L. Knopoff, Observations of multiple seismic events, Bull. Seism. Soc. Am., 54, 19, 1964.

Pomeroy, P. W., G. Hade, J. Savino, and R. Chander, Preliminary results from the high gain, wide-band, long-period electro-magnetic seismograph systems, J. Geophys. Res. 74, 3295, 1969.

Press, F., Seismic wave attenuation in the crust, J. Geophys. Res., 64, 565, 1959.

Press, F. and S. Biehler, Inferences on crustal velocities and densities from P wave delays and gravity anomalies, J. Geophys. Res., 69, 2979, 1964.

Prodehl, C., Seismic refraction studies of crustal structure in Western United States, Bull. Geol. Soc. Am., 81, 2629, 1970.

Reiter, L., An investigation into the time term method in refraction seismology, Bull. Seis. Soc. Am., 60, 1, 1970.

Ringwood, A. E., Mineralogy of the mantle, in Advances in Earth Science, ed. by P. M. Hurley, M.I.T. Press, Cambridge, 357, 1964.

Savarensky, Ye. F., T. A. Proskuryakova, V. B. Glasko, Ya, Sh. Granit, and Ye. V. Voronina, Lateral refractions of Rayleigh waves from earthquakes and microseisms in the North Atlantic, Bull. Acad. Sci. USSR, Geophys. Ser. English Transl., no. 2, 100, 1969.

Sato, R., Attenuation of seismic waves, Jour. Phys. Earth, 15, 32, 1967.

Sclater, J. G., and J. Francheteau, The implications of terrestrial heat flow observation on current tectonic and geochemical models of the crust and upper mantle of the earth, Geophys. J., 20, 509, 1970.

Seidl, D., St. Müller, and L. Knopoff, Dispersion von Rayleigh-wellen in Sudwestdeutschland und in den Alpen, Geophys., 32, 472, 1966.

Sellevol, M. A., and R. E. Warrick, A refraction study of the crustal structure in Southern Norway, Bull. Seism. Soc. Amer., 61, 457, 1971.

Smith, S. W., A reinterpretation of phase velocity data based on the Gnome travel time curves, Bull. Seism. Soc. Am., 52, 1031, 1962.

Solomon, S. C., Seismic attenuation and the state of the upper mantle, Ph.D. thesis, Massachusetts Institute of Technology, Cambridge, 321 pp. 1971.

Solomon, S. C., and M. N. Toksoz, Lateral variation of attenuation of P and S waves beneath the United States, Bull. Seism. Soc. Am., 60, 819, 1970.

Spetzler, H., and D. L. Anderson, The effect of temperature and partial melting on velocity and attenuation in a simple binary system, J. Geophys. Res., 73, 6051, 1968.

Stacey, F. D., Physics of the Earth, 324 pp., John Wiley and Sons, New York, 1969.

Sutton, G. H., W. Mitronovas, P. W. Pomeroy, Short-period seismic energy radiation patterns from underground nuclear explosions and small-magnitude earthquakes, Bull. Seism. Soc. Am., 57, 249, 1967.

Takeuchi, H., J. Dorman, and M. Saito, Partial derivatives of surface wave phase velocity with respect to physical parameter changes within the earth, J. Geophys. Res., 69, 3429, 1964.

Teng, T. L., Attenuation of body waves and the Q structure of the mantle, J. Geophys. Res., 73, 2195, 1968.

Tsai, Y. B., and K. Aki, Simultaneous determination of the seismic moment and attenuation of seismic surface waves, Bull. Seism. Soc. Am., 59, 275, 1969.

Wagner, H. M., Linear programming techniques for regression analysis, J. Amer. Stat. Assoc., 54, 206, 1959.

Walsh, J. B., Attenuation in partially melted material, J. Geophys. Res., 73, 2209, 1968.

Walsh, J. B., A new analysis of attenuation in partially melted rock, J. Geophys. Res., 74, 4333, 1969.

Weichert, D. H., Upper mantle structure under the Churchill province of the Canadian Shield, east of the Yellowknife seismic array, Jour. Phys. Earth, 16, 93, 1968.

Wetmiller, R. J., An earthquake swarm on the Queen Charlotte Islands fracture zone (abstract), Earthquake Notes, 41, 13, 1970.

Wickens, A. J., and K. Pec, A crust-mantle profile from Mould Bay, Canada, to Tucson, Arizona, Bull. Seism. Soc. Amer., 58, 1821, 1968.

Zener, C. M., Elasticity and Anelasticity of Metals, University of Chicago Press, Illinois, 170 pp., 1948.

APPENDIX

FOURIER TRANSFORMS: FAST, DISCRETE, AND CONTINUOUS

The fast Fourier transform, or FFT (Cooley and Tukey, 1965) is an efficient method for computing the discrete Fourier transform. The discrete Fourier transform, or DFT may be defined by

$$A(k) = \sum_{n=0}^{N-1} X(n) \exp(-i 2\pi nk/N) \qquad k=0,1,\ldots,N-1 \qquad (1)$$

$$\text{where } X(n) = \frac{1}{N} \sum_{k=0}^{N-1} A(k) \exp(+i 2\pi nk/N) \qquad n=0,1,\ldots,N-1 \qquad (2)$$

A(k) is the kth coefficient (usually complex) of the DFT and X(n) is the nth sample of an equally spaced time function. The spacing between each sample is Δ t while the spacing between each coefficient of the DFT is Δf or $1/(N\Delta t)$. X(n) is a discrete periodic function of time whose fundamental period is $N\Delta$ t. A(k) is the discrete periodic amplitude spectrum of X(n) whose fundamental period in the frequency domain is $N\Delta$f. In equation (1) and equation (2) $\exp(-i2\pi nk/N)$ is equivalent to $\exp(-i\omega_k t_n)$ where $\omega_k = \frac{2\pi k}{N\Delta t}$ and $t_n = n\Delta t$ are discrete angular frequencies and discrete times.

The surface wave train recorded on a seismogram is a continuous non periodic function of time whose true representation in the frequency domain is the continuous Fourier transform

$$A(\omega) = \int_{-\infty}^{+\infty} f(t) \exp(-i\omega t)\, dt$$

$$\text{where} \qquad f(t) = \frac{1}{2\pi} \int_{-\infty}^{+\infty} A(\omega) \exp(+i\omega t)\, d\omega$$

A(k) can be used to approximate $A(\omega)$ if it is multiplied by Δt (Cooley et al., 1967; Brigham and Morrow, 1967). This approximation only

holds when $0 \leq$ frequency $\leq N\Delta f/2$, $N\Delta f/2$ being the Nyquist frequency.

The spectral resolution of the fast Fourier transform or the number of coefficients A(k), computed per cycle per second, is determined by Δf or $1/N\Delta t$. By increasing $N\Delta t$ we can decrease Δf and cause the FFT to reflect more directly frequencies it otherwise would have masked. For a given number data points we can increase N by adding on data points equal to zero (Bergland, 1969). The final number of data points, however, must be expressable as 2^n, where n is a whole, positive number. When data points equal to zero are added, and the FFT is used to approximate the continuous Fourier transform, we need not use additional normalization procedures since the time function f(t) is assumed to be zero before and after the actual signal.